Nat. Hazards Earth Syst. Sci., 23, 2475–2504, 2023
https://doi.org/10.5194/nhess-23-2475-2023

Natural Hazards and Earth System Sciences
Open Access
EGU

Climate-induced storminess forces major increases in future storm surge hazard in the South China Sea region

Melissa Wood[1], Ivan D. Haigh[1], Quan Quan Le[2], Hung Nghia Nguyen[2], Hoang Ba Tran[2], Stephen E. Darby[3], Robert Marsh[1], Nikolaos Skliris[1], Joël J.-M. Hirschi[4], Robert J. Nicholls[5], and Nadia Bloemendaal[6]

[1]School of Ocean and Earth Science, National Oceanography Centre Southampton, University of Southampton, Waterfront Campus, European Way, Southampton, UK
[2]Southern Institute of Water Resources Research (SIWRR), 658th Vo Van Kiet Avenue, Ward 1, District 5, Ho Chi Minh City, Vietnam
[3]School of Geography and Environmental Science, University of Southampton, Highfield, Southampton, UK
[4]National Oceanography Centre, European Way, Southampton, SO14 3ZH, UK
[5]Tyndall Centre for Climate Change Research, University of East Anglia, Norwich, UK
[6]Institute for Environmental Studies (IVM), Vrije Universiteit Amsterdam, 1081 HV, Amsterdam, the Netherlands

Correspondence: Ivan D. Haigh (i.d.haigh@soton.ac.uk)

Received: 19 December 2021 – Discussion started: 17 January 2022
Revised: 23 April 2023 – Accepted: 19 May 2023 – Published: 13 July 2023

Abstract. Coastal floods, driven by extreme sea levels, are one of the most dangerous natural hazards. The people at highest risk are those living in low-lying coastal areas exposed to tropical-cyclone-forced storm surges. Here we apply a novel modelling framework to estimate past and/or present and future storm-surge-level and extreme-sea-level probabilities along the coastlines of southern China, Vietnam, Cambodia, Thailand, and Malaysia. A regional hydrodynamic model is configured to simulate 10 000 years of synthetic tropical cyclone activity, representative of a past/present (1980–2017) and high-emission-scenario future (2015–2050) period. Results show that extreme storm surges, and therefore total water levels, will increase substantially in the coming decades, driven by an increase in the frequency of intense tropical cyclones. Storm surges along the southern Chinese and northern and southern Vietnamese coastlines increase by up to 1 m, significantly larger than expected changes in mean sea-level rise over the same period. The length of coastline that is presently exposed to storm surge levels of 2.5 m or greater will more than double by 2050. Sections of Cambodian, Thai, and Malaysian coastlines are projected to experience storm surges (at higher return periods) in the future, not previously seen, due to a southward shift in tropical cyclone tracks. Given these findings, coastal flood management and adaptation in these areas should be reviewed for their resilience against future extreme sea levels.

1 Introduction

Around the world's coastlines it is estimated that $\sim$ 230 million people are directly exposed to some level of storm surge hazard from either tropical or extra-tropical cyclone activity (SwissRe, 2017). The populations most acutely at risk of storm-surge-induced extreme sea levels are those settled on low-lying coastlines within tropical zones associated with intense tropical cyclone (TC) activity (Nicholls, 2006; McGranahan et al., 2007; Woodruff et al., 2013; Kirezci et al., 2020; Edmonds et al., 2020; Dullaart et al., 2021). Yet global assessments of flood risk regularly overlook the contribution of low-probability TC events when considering storm-surge-induced extreme-sea-level flooding (Muis et al., 2016; Dullaart et al., 2021). Furthermore, while there is considerable uncertainty regarding future changes in TC intensity and frequency, particularly at a local scale, it is thought that the risk of TC-induced storm surge flooding will increase in the future (Bloemendaal et al., 2022a). To better protect present and future coastal communities, it is vital

that we improve our understanding of local-scale TC-driven storm surge hazard and risk.

The main difficulty in assessing TC-induced storm surge hazard, both at present and into the future, is that intense TC events are, by their very nature, infrequent (Mori et al., 2019; Dullaart et al., 2021). TCs are not only rare events, but they also typically affect comparatively short stretches of coastline (< 500 km) as they approach land, and so storm surges are often underrepresented in the data from the sparsely distributed network of global tide gauges (Pugh and Woodworth, 2014; Bloemendaal et al., 2020a). Furthermore, analysing extreme storm surge behaviour, and estimating storm surge hazard, ideally requires long (50–100 years) time series of sea-level data, which do not exist in most tropical regions (Irish et al., 2011). This limitation is acutely problematic because extreme-sea-level probabilities based on short records are notoriously imprecise with large uncertainties (Irish et al., 2011; Lin and Emanuel, 2016; Kirezci et al., 2020).

To overcome these problems, previous studies have adopted two different approaches with the same goal of extending the historic or predicted future sea-level record available from existing tide gauge data. The first approach is to reconstruct multi-decadal storm surge and/or total water-level time series through the use of statistical models to infer surge time series from more widely available meteorological datasets. These methods use simple linear or multiple regression models on climate indices to reconstruct long time series of surge levels from which extreme values and trends can be more robustly estimated. This has been done at both regional and global scales, using, for example, the tide gauge record and the 20th century reanalysis dataset (Cid et al., 2018, 2017; Zhang and Wang, 2021) or a mixture of climate reanalyses data (Wahl and Chambers, 2016; Tadesse and Wahl, 2021). Statistical approaches mostly benefit from modest computational resource needs, but this advantage is traded off against the use of meteorological forcings that often have insufficient spatial resolution in tropical regions to capture the effects of cyclone activity on sea levels (Haigh et al., 2014; Cid et al., 2018).

The second approach involves the use of hydrodynamic models to generate multi-decadal time series of storm surge and extreme sea levels across oceanic domains. TC-induced storm surges are challenging to model at continental or global scales because these intense storms typically have diameters less than the model mesh resolution or are smoothed out in the large grid cells of meteorological datasets, meaning they are therefore difficult to resolve (Murakami and Sugi, 2010; Larson et al., 2014; Takagi et al., 2017; Bloemendaal et al., 2019; Kirezci et al., 2020). An earlier version of the Global Tide and Surge Model (GTSM; using ERA-Interim reanalysis data – see Dee et al., 2011) was found to underestimate TC-induced extreme sea levels for this reason. This problem was subsequently improved in the latest GTSM iteration, v3 (Muis et al., 2020), with an updated model resolution and the use of the ERA5 reanalysis meteorological dataset (Hersbach, 2020). The authors successfully simulated past/present storm surges and extreme sea levels.

To address the scarcity of adequate low-probability storm surge events within extreme-sea-level analysis, several studies have recently attempted to force numerical storm surge models with synthetic datasets that seek to represent long-term TC activity over many hundreds to thousands of years. For example, Haigh et al. (2014) extended the work of Harper et al. (2009) and generated a 10 000-year synthetic dataset of TC activity for the Australian region, which thus included extreme TCs larger than in the observational dataset but that were physically plausible. This 10 000-year atmospheric dataset was used to force a MIKE 21 hydrodynamic model of the Australian coast to estimate present-day sea-level exceedance probabilities more accurately. More recently Bloemendaal et al. (2020a) similarly developed a synthetic TC dataset called STORM (Synthetic Tropical cyclOne geneRation Model), which statistically resampled and simulated TC tracks and intensities from 38 years of historical atmospheric data from the International Best Track Archive for Climate Stewardship dataset (IBTrACS; Knapp et al., 2010) to the equivalent of 10 000 years under the same climate conditions. Dullaart et al. (2021) subsequently coupled this STORM data with the GTSMv3 model to produce past/present (1980–2018) storm surge and extreme-sea-level return period estimates for coastlines worldwide, directly tackling the problems of precision in the relative location (of tide gauges) and availability of TC storm surge data. Earlier studies, for example of Haigh et al. (2014) and Dullaart et al. (2021), focused on past/present-day extreme sea levels and did not apply the approach to look at possible future changes in TC activity with climate change.

Looking to the future, coastal flood hazard is expected to increase, primarily due to rising relative mean sea level but also due to changes in storm surges driven by changes in the frequency, intensity, and tracks of tropical and extra-tropical cyclones (Kirezci et al., 2020) and change in tides (Haigh et al., 2020). Note, wave setup and runup are also likely to be important in some regions, but as discussed later, for simplicity we ignore the influence of waves in this paper. To date, a large number of studies has focused on assessing changes in global mean sea levels. Much less research has been devoted to determining the contribution of climate-driven changes in storm activity in forcing extreme storm surges (Fox-Kemper et al., 2021). While there is consensus that there will be substantial changes to the frequency and severity of tropical (and extra-tropical/mid-latitude) cyclones in the future (Mousavi et al., 2011; Woodruff et al., 2013; Wahl et al., 2017; Knutson et al., 2020; Emanuel, 2021), the two most recent reports of the Intergovernmental Panel on Climate Change (IPCC) underscore that there is currently "low confidence" ($\sim 20\,\%$ chance) in our ability to correctly predict how climate-driven storm surges may contribute to changes in future sea-level extremes (Wong et al., 2014; Fox-Kemper et al., 2021). This

deep uncertainty arises not only from the small number of studies assessing changes in storm surge available at the time of the last IPCC assessment review, but also from the significant challenge of predicting changes in tropical (and mid-latitude) cyclone activity at a local and regional scale.

Studies to date have also assumed that storm surge extreme behaviour has been, and will continue to be, stationary in the future (Hinkel et al., 2014; Vitousek et al., 2017). But with projections of a changed climate by the end of this century, this hypothesis has been challenged in recent modelling studies (Lin-Ye et al., 2020; Tadesse and Wahl, 2021). For European coastlines, modelling shows that by 2100 extreme storm surge levels may augment relative sea-level rise by over 30 % under mean Share Socioeconomic Pathway 5-8.5 (SSP5-8.5) climate projections (Vousdoukas et al., 2016). More recently Calafat et al. (2022) examined tide gauge observations from 1960 to 2018 for northwestern European seas and discovered statistically significant past changes in storm surge extremes due to climate variability and anthropogenic forcing over this period. This trend has already affected the likelihood of surge extremes in this region and is likely to be magnified in the future. Since existing coastal flood defences were originally designed under the presumption of stationary surge extremes, there is the compelling question about how effective current coastal flood defences actually are now against present storm surge hazard, in this region and beyond. The issue has strong implications for not only today's coastal planning, but also future coastal planning. Thus, it is vital that we accurately assess past and future changes in storm surges and extreme sea levels, especially in areas projected to experience a shift in intense TC activity under our changing climate.

Therefore, the overall aim of this paper is to more accurately estimate both present and future storm surge and extreme-sea-level probabilities along coastlines in areas with intense TC activity. As a case study, we focus here on the densely populated coastline of southern China, Vietnam, Cambodia, Thailand, and Malaysia in Southeast Asia (Fig. 1). Southeast Asia has long been identified as a "hotspot" for projected future mean sea-level rise, plus extremes of sea levels related to TC activity (McGranahan et al., 2007; Nicholls and Cazenave, 2010; Kirezci et al., 2020; Nicholls et al., 2021). Of the most densely populated metropolitan areas at risk from storm surges around the world, 8 out of 10 are located in Southeast Asia (SwissRe, 2017), and 4 of those 8 are located within our proposed study area (Ho Chi Minh City (14), Pearl River Delta (near 4), Shantou (near 3), and Manila (near 26) in Fig. 1). The study area sits within the western North Pacific (WNP) TC region, which currently accounts for almost one-third of all TC counts globally (Gray 1975, 1977). WNP TCs (typhoons in this region) are projected to become more intense over the course of the 21st century, with higher-category cyclones increasing in frequency (Chan, 2005; Zang and Church, 2012; Emanuel, 2013; Woodruff et al., 2013; Lap, 2019; Knutson et al., 2020; Emanuel, 2021; Bloemendaal et al., 2022a). Within the study area, a key interest is the coastline of Vietnam, as this is the area of focus of the project that funded this study. More than 70 % of Vietnam's population lives in coastal regions (GFDRR, 2015), with a large proportion residing in one of its two deltas – the Red and Mekong River deltas (Fig. 1). These delta communities are especially vulnerable to flooding because the low-lying land is densely populated and rich in infrastructure and high-value assets, with a river able to funnel storm surges further inland.

The specific objectives and structure of the paper is as follows. As a first objective, we configure a depth-averaged hydrodynamic model of the South China Sea and extensively validate it against measured sea-level data from tide gauges in the region. A description of the hydrodynamic model and validation exercise is provided in Sect. 2. As a second objective, we force the hydrodynamic model with 10 000 years of TC activity for the past/present (1980–2017) and future (2015–2050; based on a high-emission scenario), from the novel synthetic STORM dataset of Bloemendaal et al. (2020b, 2022b). From the model outputs, we estimate past, present, and future storm surge and extreme-sea-level probabilities along the coastlines of southern China, Vietnam, Cambodia, Thailand, and Malaysia. The approach we take to simulate the storm surges and calculate the associated extreme probabilities is described in Sect. 3. As a third objective, we compare the past and future probabilities, first for just the storm surge component and then for total water levels (i.e. storm surge plus astronomical tide). The results of this comparison are described in Sect. 4. As a sub-objective, we also examine the tracks of the cyclones that are responsible for generating the largest storm surges in particular locations along the coastline of the case study area. The key findings are discussed in Sect. 5, and conclusions are given in Sect. 6.

2 The hydrodynamic model configuration and validation

We start this section off by describing the configuration of the hydrodynamic model (Sect. 2.1). We then discuss the model validation against observations, first for the astronomical tidal component (Sect. 2.2) and then for storm surges and total water levels (Sect. 2.3).

2.1 Model configuration

We configured a depth-averaged (i.e. barotropic) hydrodynamic model of the South China Sea using the Danish Hydraulic Institute's MIKE 21 FM (flexible mesh) suite of modelling tools (DHI, 2017a). The MIKE 21 FM model uses the solution of the incompressible Reynolds-averaged Navier–Stokes equations, utilising the assumptions of Boussinesq and hydrostatic pressure. The spatial discretisation of the primitive equations is performed using a cell-centred finite-volume method. The MIKE 21 FM model uses an irregular

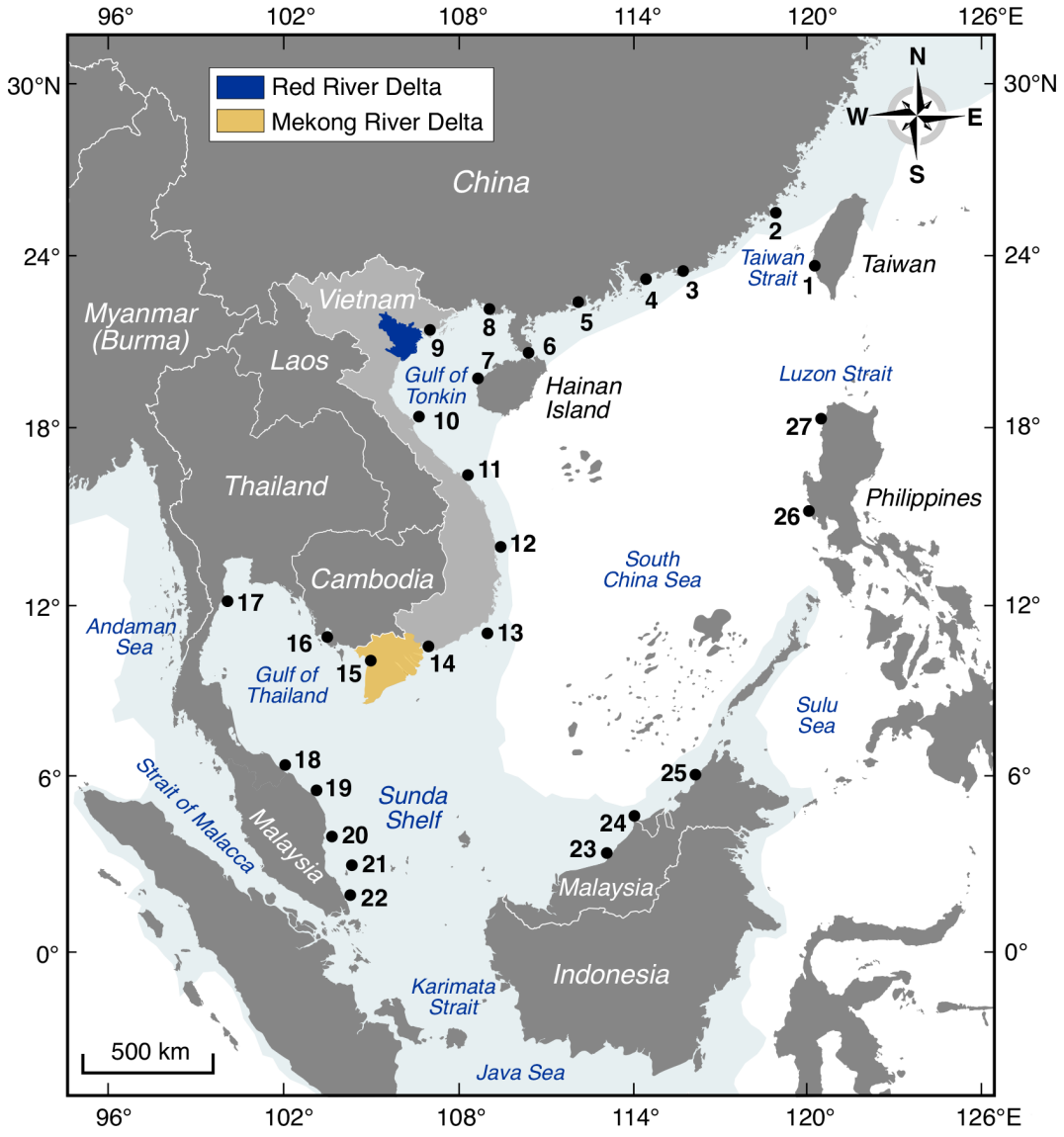

Figure 1. South China Sea model domain, with the location of tidal gauges numbered (also see Table 1) and the location of the Red and Mekong River deltas highlighted. The shaded blue area, in the sea, shows the approximate coverage of the continental shelf, at ∼ 250 m depth.

triangular mesh to represent the domain area. This provides computation efficiencies by optimising element size to range from coarse resolution for deep ocean to a more precise representation around detailed coastlines or for features of interest. We describe each step of the model configuration below. In addition, a schematic giving an overview of the model configuration steps and data inputs is provided in Appendix A, Fig. A1.

The model grid we created for the South China Sea is shown in Fig. 2a. It extends from approximately 3° S and 100 to 120° W to 25° N. It encompasses the east coast of Malaysia and Thailand, the entire coast of Cambodia and Vietnam, and extends to southern China. We developed the model off the continental shelf of these countries with the eastern domain of the model running along the coastline of Borneo, Malaysia; Brunei; the Philippines; and Taiwan (Fig. 1). The model grid has seven open sea tidal boundaries, shown in red in Fig. 2a. The model mesh reduces from ∼ 52 km at the open sea boundaries to approximately ∼ 2 km along parts of the coast. Along our study coastline (the grid cells shown in green in Fig. 2a), the model mesh reduces in resolution from ∼ 11 km along southern China and Malaysia to ∼ 5 km around Hainan Island and along the coast of Thailand and China, down to ∼ 2 km along the Vietnam coastline (as mentioned above, we focus on Vietnam, as this is the central region of interest in the project that funded this study).

We are aware that some global hydrodynamic models (such as GTSMv3; Muis et al., 2020) now have a resolution along the coast of finer than 2 km, and we could have increased the coastal resolution further. However, we purposely did not go to a finer resolution because (1) our study involved running the model almost 100 000 times for synthetic cyclones – increasing the resolution would significantly increase total run-time, and (2) our model design should consider our Vietnamese co-authors' objective to potentially use the model for future studies, without having regular access to a supercomputer. Therefore, we wanted the model to be easy to run on a standard desktop computer.

To define the coastal land boundary of the model mesh, we used the Global Shoreline dataset from the National Geospatial Intelligence Agency, obtained via the National Oceanic and Atmospheric Administration (https://shoreline.noaa.gov, last access: 19 September 2020). For bathymetry, we used the 15 arcsec resolution global dataset from SRTM15+ (v2). This bathymetry data were downloaded from the Scripps Institution of Oceanography website (https://topex.ucsd.edu, last access: 19 September 2020; Tozer et al., 2019) and interpolated onto the model grid. All model data therefore are measured using an EGM96 vertical reference datum. The interpolated model bathymetry is shown in Fig. 2b.

To generate the astronomical tidal component, we forced the open model boundaries with tidal levels derived from the Oregon State University Tidal Inversion Software (OTIS), TPXO (Egbert and Erofeeva, 2002; Martin et al., 2009). The tidal harmonic constituents were downloaded from the OSU TPXO Tide Models website (https://www.tpxo.net/, last access: 7 September 2020) for points along the seven open sea boundaries of our model, using OTIS regional "China Seas and Indochina" region model at $1/30^\circ$ resolution. The data are provided for eight primary (M2, S2, N2, K2, K1, O1, P1, Q1), two long period (Mf, Mm), and three non-linear (M4, MS4, MN4) harmonic constituents. With these data, the tide was then predicted, for each boundary grid point, using the Tidal Model Driver (TMD) MATLAB toolbox (https://www.esr.org/research/polar-tide-models/, last access: 9 September 2020; Erofeeva et al., 2020), which has been designed specifically to predict tidal levels from OTIS-formatted harmonic constituents. We also accounted for direct gravitational forcing in the model simulations by including the "tidal potential" forcing incorporated within MIKE 21 FM (DHI, 2017a). Note that we forced the model with astronomical tides for the validation exercise (see Sect. 2.2 and 2.3), but when running the TC simulations (Sect. 3), we ran surge-only simulations, switching off the tidal forcing.

For bed friction the MIKE 21 FM model uses Manning's formula, and we used the model's default roughness coefficient value $32\,m^{1/3}\,s^{-1}$. The overall discrete model time step was set to 3600 s (i.e. 1-hourly); however the MIKE 21 FM hydrodynamic module, which resolves the shallow water equations over the model domain, uses a variable time step to ensure stability of the model during the simulation. This means that time steps would reduce further (between 0.01 and 25 s) as necessary, between outputs, to ensure optimal time integration and space discretisation solutions. For all other settings (e.g. eddy viscosity), we use the default MIKE 21 FM settings. A schematic of the basic model configuration is also provided in Appendix A, Fig. A1.

2.2 Model validation of astronomical tides

We undertook two validation exercises to ensure that our MIKE 21 FM hydrodynamic model accurately captures the complex tidal, storm surge, and total water-level (tide plus storm surge) characteristics of the study region. In this section we describe the first validation, which focuses on just the astronomical tidal component (Appendix A, Fig. A2(2d)). The South China Sea has complex tidal characteristics, with some regions experiencing semi-diurnal tides, some mixed, and other regions experiencing strong diurnal tides with varying tidal ranges (Phan et al., 2019).

We obtained measured sea-level data, at hourly frequency, at 27 tide gauge stations located around the South China Sea model domain, from the University of Hawaii Sea Level Center (https://uhslc.soest.hawaii.edu, last access: 18 March 2020; Caldwell et al., 2015). The locations of the tide gauge sites are shown numbered in Fig. 1 and listed in Table 1. Extra years of sea-level data at four of these tidal gauge sites (Phu Quoc, Phu Quy, Son Tra, and Rach Gia) were also made available directly from the Southern Institute of Water Resources Research in Vietnam. Despite there being a good number of tide gauges around the South China Sea region, only a third have 30 or more years of data, and several sites have very short records (Table 1). To remove the major meteorological influences and extract just the astronomical component and to overcome the problem of an incomplete data record at some tide gauge locations, we undertook a harmonic analysis on the available observed levels using the MATLAB T-Tide tidal analysis software (Pawlowicz et al., 2002). We obtained the standard set of 67 tidal constituents, for the most recent year with the least amount of missing data. We then used MATLAB T-Tide software again, with the extracted harmonic constituents, to predict the tide, hourly, for January 2019. We chose the year 2019 because 2019 had the most completed measured records across the 27 sites. At each tide gauge site, we calculated the annual mean sea-level value in 2019 and then subtracted this level from the data to offset each time series so it was equivalent to the model datum of m.s.l.

We then ran the hydrodynamic model for January 2019 (including 2 d of warming period prior to the start of January 2019), forcing the model at the boundary conditions with the OTIS-derived tidal level and no meteorological forcing. Hourly results were output for the model grid points located closest to the 27 tide gauge sites. The resulting time series of model-simulated (red line) and observed tide levels (blue line) are shown in Fig. 3 for six select gauge sites along the

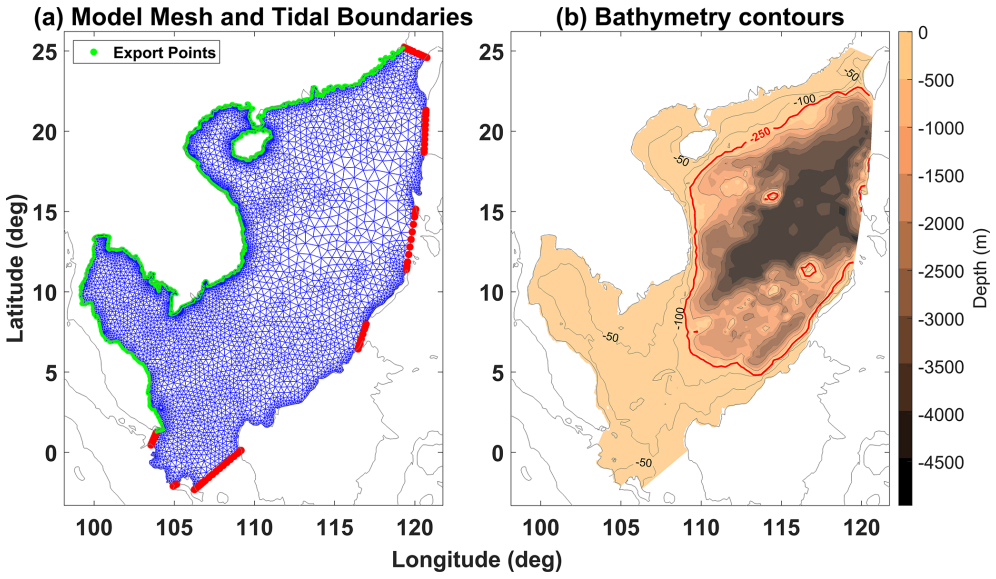

Figure 2. (a) MIKE 21 FM model mesh for the South China Sea. The irregular triangular mesh grid (blue) of the model has tidal boundaries shown in red. The coastline points exported from the model for analysis are also shown (green). **(b)** SRTM15+ ocean bathymetry for our South China Sea domain, showing nearshore −50 and −100 m contours as well as the −250 m depth contour (red) approximating the edge of the continental shelf.

Vietnamese coastline (sites 10 to 14, Fig. 1). It is clear that at these six locations and the other sites (not shown) the model does an excellent job of reproducing the complex tidal dynamics of the study area. For example, the model effectively captures the transition from diurnal tides along the northern Vietnamese coast (sites 10–13) to semi-diurnal tides, with a larger range around the Mekong Delta in southern Vietnam (site 14), and then back to smaller diurnal tides on the west side of the south coast of Vietnam (site 15). Overall, the observed tidal characteristics are captured well across all 27 sites.

To quantify the difference between measured and predicted tides, we calculated the mean absolute error (MAE), the standard deviation around this MAE, and the correlation coefficient between time series for all 27 tide gauge sites. These validation statistics are listed in Table 1. Across all 27 sites, the average MAE is 0.15 m, and the mean standard deviation of the MEA is 0.1 m. The parts of the model with the largest MAE errors are typically located at sites with diurnal tides, around the Gulf of Tonkin (sites 6–9 in Fig. 1), and the smallest errors are for sites with semi-diurnal to mixed tides around the Vietnamese, Bornean, and southern Chinese coastlines (sites 1–5, 10–16, 18–26 in Fig. 1). The correlation coefficients range between 0.77 and 0.98 with the highest correlations in the northern and eastern areas of the model that experience fully or mainly semi-diurnal tidal regimes. The magnitude of differences between the measured and predicted tide is consistent with other past hydrodynamic modelling studies (e.g. Haigh et al., 2014; Muis et al., 2016; Vousdoukas et al., 2016) and highlights again that the model does accurately reproduce tidal characteristics across the model domain.

At each of the 27 tide gauge sites we also computed and compared the amplitude and phase differences of the four main tidal constituents, extracted from the model simulation and measured time series using T-Tide. The mean absolute amplitude and phase errors of the four main tidal constituents, averaged across all 27 tide gauge sites, are listed in Table 2. The mean absolute amplitude error of the four main tidal constituents are 0.05, 0,03, 0.06, and 0.06 m for M_2, S_2, O_1, and K_1, respectively. There is a slight amplitude underestimation where there are transitioning tidal regimes, such as the amplitude of larger semi-diurnal tides around the Taiwan Strait (Xiamen) and mixed diurnal tides around the Gulf of Tonkin. The mean absolute phase error of the M_2, S_2, O_1, and K_2 constituents are 17, 18, 11, and 12°, respectively. Small semi-diurnal (M_2 and S_2) phase differences exist in the model for tide gauges located around the mixed (mainly diurnal) tide zones of central Vietnam. Phase and amplitude errors may be due to the absolute decimal accuracy of some tide gauge location coordinates as much as due to model limitations. Overall, the results from this validation exercise show that the model is accurately reproducing tidal characteristics (both in terms of form and range and individual constituents) across the study domain.

2.3 Model validation of storm surges and total water levels

In this section we describe the second validation exercise, in which we assess the model's ability to accurately simulate

Table 1. Validation of tidal level output by the model. Mean absolute difference errors (mean absolute error – MAE) between modelled and observed tide gauge data, for January 2019, at each gauged location in Fig. 1. The standard deviation around this MAE is also given.

Tide gauge	ID (Fig. 1)	Latitude (degrees)	Longitude (degrees)	Date range [number of years of data available]	Mean absolute error (MAE, m)	Standard deviation of MAE (m)	Correlation coefficient
Kaohsiung	1	22.61	120.28	1980–2016 [37]	0.07	0.05	0.95
Xiamen	2	24.42	118.30	1954–1997 [28]	0.29	0.20	0.97
Shanwei	3	22.65	115.30	1975–1997 [23]	0.10	0.08	0.95
Hong Kong	4	22.27	114.38	1962–2018 [33]	0.13	0.11	0.93
Zhapo	5	21.50	111.78	1975–1997 [23]	0.12	0.09	0.97
Haikou	6	20.02	110.28	1976–1997 [22]	0.24	0.17	0.77
Dongfang	7	19.10	108.62	1975–1997 [23]	0.16	0.12	0.94
Beihai	8	21.48	108.98	1975–1997 [23]	0.20	0.13	0.98
Hon Dau	9	20.67	106.82	1995 [1]	0.32	0.25	0.89
Vung Ang	10	18.18	106.35	1996–1997 [2]	0.21	0.14	0.81
Son Tra	11	16.10	108.22	2009 [1]	0.09	0.07	0.96
Qui Nhon	12	13.77	109.38	1994–2018 [22]	0.16	0.13	0.85
Phu Quy	13	10.52	108.93	2008–2009 [2]	0.20	0.14	0.87
Vung Tau	14	10.34	107.01	1980–2018 [39]	0.18	0.12	0.97
Rach Gia	15	9.99	105.07	1996–2018 [23]	0.12	0.09	0.84
Phu Quoc	16	10.22	103.97	2008–2009 [2]	0.08	0.06	0.91
Ko Lak	17	11.79	99.90	1985–2018 [34]	0.15	0.09	0.93
Geting	18	6.25	102.12	1986–2015 [30]	0.13	0.08	0.86
Cendering	19	5.26	103.23	1984–2015 [32]	0.16	0.11	0.92
Kuantan	20	3.97	103.44	1983–2015 [33]	0.19	0.12	0.93
Tioman	21	2.81	103.60	1985–2015 [31]	0.18	0.13	0.93
Sedili	22	1.93	104.18	1986–2015 [30]	0.19	0.13	0.90
Bintulu	23	3.45	113.03	1992–2015 [24]	0.13	0.09	0.95
Miri	24	4.39	113.90	1992–2014 [23]	0.08	0.06	0.97
Kota Kinabalu	25	5.98	116.07	1987–2015 [29]	0.14	0.11	0.93
Subic Bay	26	9.75	118.30	2007–2018 [12]	0.07	0.06	0.96
Currimao	27	14.76	120.00	2009–2018 [10]	0.05	0.04	0.97

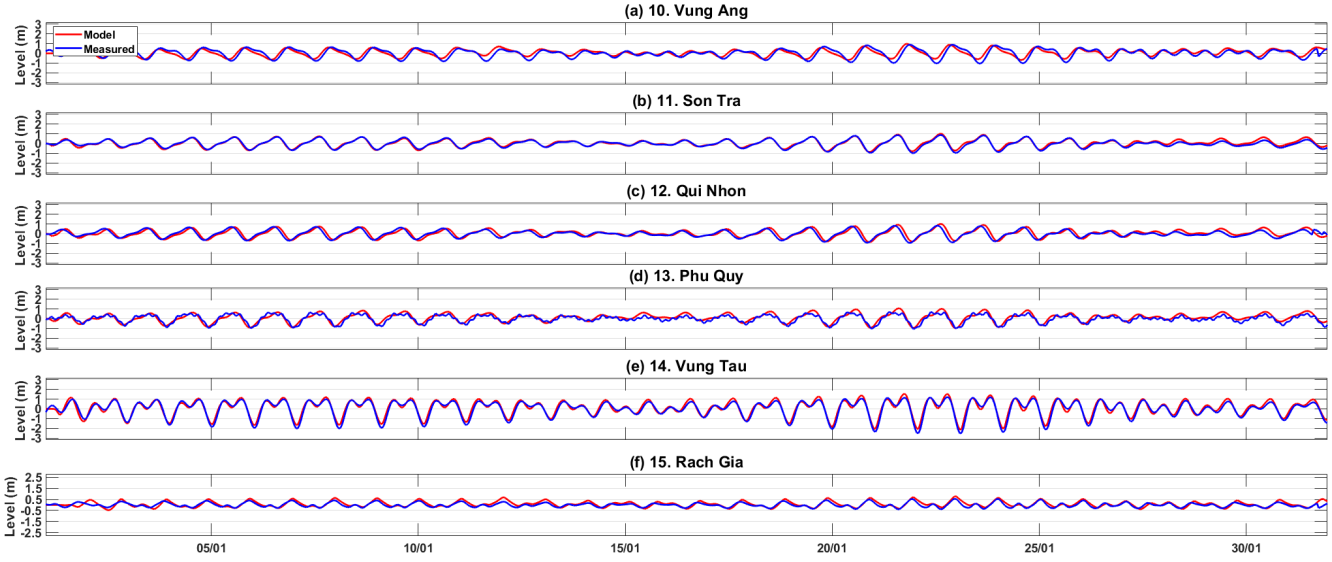

Figure 3. Comparison of modelled (red) and measured (blue) astronomical tidal time series (January 2019) at six Vietnamese tide gauge station locations (see Fig. 1 for locations).

Table 2. Mean absolute amplitude and phase errors of the four main tidal constituents for the 27 validation tide gauge sites.

Tidal constituent	Mean absolute amplitude error (m) [SD]	Median absolute phase error (degrees) [SD]
M_2	0.05 [0.04]	16.8 [15]
S_2	0.03 [0.02]	18.4 [17]
O_1	0.06 [0.06]	11.3 [7]
K_1	0.06 [0.06]	[9]

storm surges induced by TCs, and corresponding total water levels (astronomical tide plus storm surge). The length of measured sea-level data available, as already indicated and illustrated in Table 1, is on average short across the 27 gauge sites located within this study area. Consequently, only a small selection of large storm surge events are represented in the available tide gauge records. We therefore focused on those select past cyclone events for validation. A schematic of the process is given in Appendix A, Fig. A2(1).

The first step was to identify potential significant TC-driven storm surge events in the South China Sea that we could simulate and for which we could derive wind and atmospheric fields to force the model. To do this we used data from the IBTrACS version 4 TC database (https://www.ncdc.noaa.gov/ibtracs/, last access: 06 January 2021; Knapp et al., 2010). We collated all the TCs in IBTrACS, for the WNP region and for the period 1970 to 2020, which (1) made landfall, (2) have matching measured sea-level data at a tide gauge close to the landfall location, and (3) capture the storm surge in the measured records for that event. Unfortunately, radius to maximum wind information was only available in the IBTrACS data for certain cyclones, and this therefore further reduced the possible number of TCs we could use for validation (as we require information on radius to maximum winds to drive an empirical wind and atmospheric pressure model; see below). Only four TC events with significant measured storm surges matched the above criteria, namely (1) Typhoon Sally in September 1996, (2) Tropical Storm Linda in October and November 1997, (3) Typhoon Ketsana in September 2009, and (4) Typhoon Mangkhut in September 2018. These cyclones impacted different stretches of coastline and thus provided a range of events suitable for validation of the model.

To simulate these four TC events, the second step was to create spatially and temporally varying wind and atmospheric pressure fields to force the hydrodynamic model. We forced the model with two different meteorological fields and compared the results. First, we used u and v wind and m.s.l. atmospheric pressure fields directly from the ERA5 reanalysis dataset (Hersbach et al., 2020). These were downloaded from the Copernicus Climate Data Store (https://cds.climate.copernicus.eu/, last access: 28 January 2020), for the known cyclone dates, on a regular $0.25° \times 0.25°$ grid at hourly resolution (Hersbach et al., 2020). These data were simply clipped to the area of interest and imported into a MIKE 21 FM grid file format with no other modification. As discussed in the Introduction, ERA5 may not accurately capture the intensity and track of TCs, due to its spatial resolution. Hence, we also derived a second set of meteorological fields for each of the four chosen storms. In this instance, we derived spatially and temporally varying wind and atmospheric pressure fields using the empirical approach of Holland (1980). To do this, we used the Cyclone Wind Generation toolbox (DHI, 2017b) built within MIKE 21 FM. To generate the empirical wind and pressure fields, we inputted the track of each of the four selected TCs at 3-hourly time steps, as captured in the IBTrACS database, along with central atmospheric pressure and radius to maximum wind values. We selected the single vortex Holland option within the toolbox, which creates an estimate of the Holland B parameters using the Holland formula specified in Harper and Holland (1999). This tool therefore generated u and v wind and pressure files for each of the four TC events on a $0.25° \times 0.25°$ grid resolution to match ERA5 spatial grid resolution for fair comparison.

The third step was to run the model to simulate behaviour for each of the four TC events. For each TC, we ran the model three times. First, we ran the model forced with the wind fields derived from ERA5 and second forced with the empirical wind fields derived from the Holland model. For each TC, we also ran the model a third time, with just astronomical tidal forcing at the open boundaries (i.e. no meteorological forcing) so that we could isolate the storm surge components in the wind-forced simulations. A schematic of this storm surge validation procedure is given in Appendix A, Fig. S2(a–c). For each simulation, we ran the model for approximately 5 d around the event; this included 2 d of warm up a day before the event, the day of the event, and a day after the event. We then finally, for each of the four TCs, visually compared the simulation results against the measured record, at the tide gauge closest to where the TC made landfall. To quantify the difference between predicted and measured total water levels and storm surges, we calculated the MAE between modelled and measured time series for these four TC events (Table B1, Appendix B).

A plot of model-simulated (red line) and observed (blue line) total water level and storm-surge-only time series is shown in Fig. 4a and b, respectively, for TC Ketsana. TC Ketsana made landfall close to the tide gauge at Son Tra, Vietnam (site 11 in Fig. 1), in September 2009, producing a storm surge of approximately 1.4 m. Results for the other three TC events are shown in Appendix B (Figs. B1, B2, and B3). For each of the four TC events used in this validation, it is clear that the simulations driven with ERA5 wind data significantly underestimate the magnitude of the storm surge and hence total water levels. However, for all four TC events, the model simulations driven with wind and pressure forcing derived from the empirical Holland model do a better

job of reproducing the overall magnitude of the storm surge and total water level. The MAEs for each of the four TC events' total water level and storm surge are similarly listed in Table B1 in Appendix B (for both the simulations driven by ERA5 meteorological fields and the simulations driven by the empirical Holland model results). When the ERA5-derived forcing fields are used, the MAEs vary between 0.17 and 0.26 m for storm surge and 0.24 and 0.32 m for total water level but reduce between 0.08 and 0.17 m for storm surge and between 0.15 and 0.29 m for total water level when the empirical forcing fields are used in the model. Overall, these validation findings provide confidence that the hydrodynamic model is able to accurately capture both total water levels and the storm surge component of TC events when the empirical Holland meteorological forcing approach is used to generate wind and pressure fields for the hydrodynamic model.

3 Approach for simulating present and future extreme sea levels

In this section we start by describing the 10 000-year TC database, representative of the past/present and future high-emission scenario (Sect. 3.1). Then we detail how we force the validated hydrodynamic model with these 10 000-year datasets of TC activity (Sect. 3.2). Finally, we discuss how we estimate both past/present and future storm surge and extreme-sea-level probabilities along the coastlines of southern China, Vietnam, Cambodia, Thailand, and Malaysia from the model simulations (Sect. 3.3).

3.1 Synthetic tropical cyclone datasets

To estimate extreme storm surges and total water levels along our study coastline, we utilised synthetic TC data from the STORM database. Bloemendaal et al. (2020a) developed and applied the STORM algorithm to TCs from 38 years of historical IBTrACS data (1980–2018) to statistically extend the original record to the equivalent of 10 000 years of TC activity and create the original past/present STORM database. The STORM dataset preserves the TC statistics found within the original 38-year dataset. STORM was developed to mimic the seasonality of the observed data it uses, so for TCs in southeastern Asia genesis occurs between May and November. The STORM database therefore provides 3-hourly, seasonally appropriate information on an individual cyclone's location, wind speed, pressure, radius to maximum winds, and storm category. Further details are available in Bloemendaal et al. (2020a).

We extracted all TCs in the WNP area that reached at least hurricane strength (category 1 or greater on the Saffir–Simpson Hurricane Wind Scale; Simpson and Saffir, 1974) from the global STORM dataset (Bloemendaal et al., 2020b). In the WNP, this amounts to 156 879 individual synthetic cyclones. We then excluded TCs that did not cross our model domain or those that were very short-lived (lasting < 9 h). This left a sub-set of 30 843 individual TCs for our study area, which we henceforth refer to as the baseline data subset.

For the future datasets we utilised the future STORM synthetic TC dataset of Bloemendaal et al. (2022a, b). They extended their original study by applying the STORM algorithm to extracted data from four high-resolution climate models, namely, CMCC-CM2-VHR4, CNRM-CM6-1, EC-Earth3P-HR, and HadGEM3-GC31-HM. Each climate model was originally run at a high spatial resolution for the period 2015–2050 and forced with emissions representative of the SSP5-8.5 high-emission climate change scenario. The SSP5-8.5 climate change scenario represents unconstrained growth in economic output and energy, which exploits abundant fossil fuel resources and relies on global markets and technological progress to achieve sustainable development (Pielke et al., 2022; IPCC, 2019). It describes a society that develops within the highest greenhouse gas emissions pathway, linked to greater reliance on adaptation, rather than mitigation, to address climate challenges. Using a so-called "delta approach", Bloemendaal et al. (2022a) utilised TCs extracted from the high-resolution climate model runs to statistically generate synthetic events representative of 10 000 years of TC activity, for each of the four future climate simulations. Results from the study indicate that the probability of intense TCs, on average, more than doubles in most regions, including the WNP. Further details on the creation of STORM data for a future climate can be found in Bloemendaal et al. (2022a). The dataset can be downloaded at Bloemendaal et al. (2022b). To see if this pattern is replicated within our study area, Table 3 gives the number of TCs in each of the four future STORM datasets that pass within the bounds of our model domain, as well as the number of TCs that pass within the bounds of the model domain for the (unfiltered) baseline STORM dataset. The table shows the number of tropical storms or depressions and category 1, 2, 3, 4, and 5 TCs in each option. The numbers do indeed reflect the global trend of a decrease overall in the number of tropical storms and depressions but an increase in the number of more intense (category 1–5 on the Saffir–Simpson scale) TCs in the future. Although, as expected, there are differences in the number of TCs between the STORM datasets also derived from the four different future climate models.

Due to the large computational expense of simulating the equivalent of 10 000 years of TC activity (and within the constraints of the budget of the study that funded this work), it was not possible to submit MIKE 21 FM model simulations for all four future climate datasets. Hence, we elected to only use data from a single future global climate model run. We selected the future STORM dataset based on the CNRM-CM6-1 climate model run because it approximately matched the average number of the most intense (categories 4 and 5) TCs across all four climate model options. We thus extracted

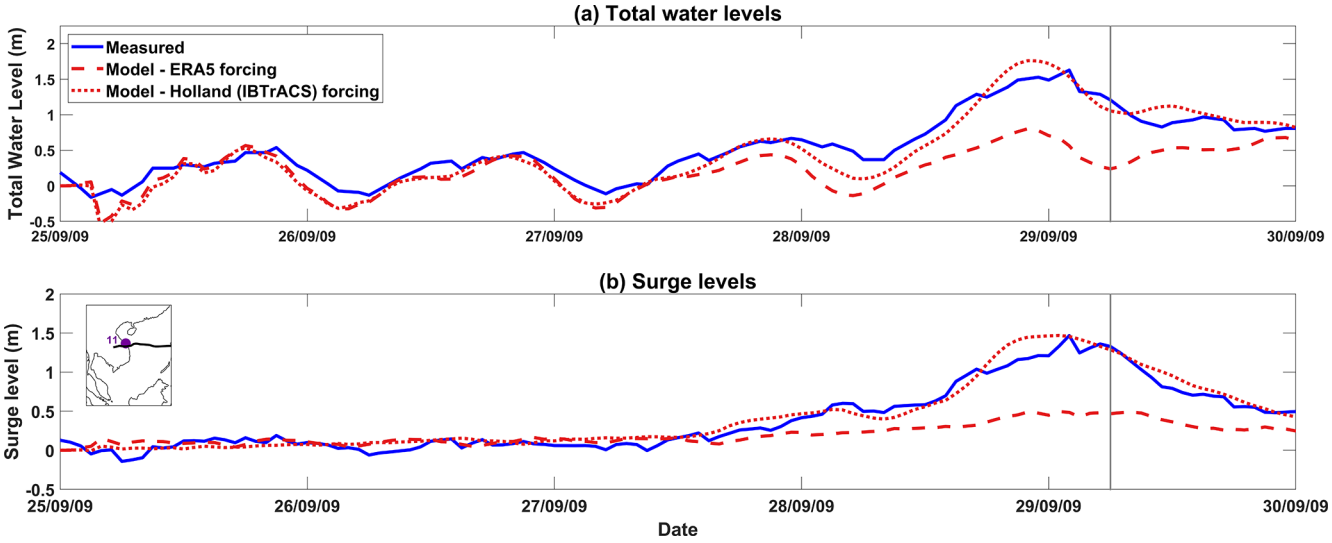

Figure 4. **(a)** Measured and modelled total water levels and **(b)** measured and modelled storm surges at Son Tra (site 11 in Fig. 1) for Typhoon Ketsana, which made landfall at approximately 06:00 UTC on 29 September 2009 (green vertical line). Modelled total water level and surges using ERA5 (red dashed) and the Holland model's (red dotted) wind and pressure fields against measured data (blue).

all future synthetic TCs from the CNRM-CM6-1 climate run, using the same filtering procedure as for the baseline dataset above (to additionally remove the short-lived TCs). This left a sub-set of 63 328 individual TCs for our study area, which we henceforth refer to as the future data sub-set.

Heat maps illustrating the resulting track density of the synthetic (filtered, sub-set) TCs passing through the bounds of the model domain, for the baseline period (representative of the period 1989–2018) and future period (representative of the period 2015–2050 with CNRM-CM6-1, SSP5-8.5 climate scenario), are shown in Fig. 5a and b, respectively. The difference between the two track densities is shown in Fig. 5c. One interesting observation is that the density of TC tracks shift southward in the future scenario (Fig. 5b), resulting in a greater number of category 1–5 TCs impacting the central Vietnamese coastline in the 35-year interval period up to 2050, and for the first time a density of TCs will reach more southern coastlines too (Fig. 5c). Equivalent heat maps were created for the remaining climate models shown in Table 3, as shown in Appendix D (Fig. D1) for comparison. These also show a projected increase in category 1–5 TCs impacting the central Vietnamese coastline over the coming decades.

3.2 Hydrodynamic model implementation

We now describe how we forced the model with wind and pressure fields derived from these 30 843 baseline and 63 328 future TCs. We generated spatially and temporally u and v wind and atmospheric pressure fields, using the approach described above in Sect. 2.3. We used the MIKE 21 FM Cyclone Wind Generation toolbox, inputted with the track of each synthetic TC at 3-hourly time steps, along with central atmospheric pressures and radius to maximum wind values, obtained from the STORM dataset. Again, we selected the single vortex Holland option, with Holland B parameters estimated using the Holland formula specified in Harper and Holland (1999), and generated u and v wind and pressure files on a $0.25° \times 0.25°$ resolution grid. This spatial resolution was sufficient to resolve the TC within these forcing files, especially as the wind and pressure files would be further interpolated in the MIKE 21 FM software to the higher resolution of the model mesh as the cyclone traverses through the model domain.

For each individual baseline and future TC, we then simulated storm surge levels using the validated MIKE 21 FM hydrodynamic depth-averaged model, described above. We ran each simulation separately, from when each synthetic TC started or entered the model grid domain to when it dissipated or exited the model domain. We decided not to run each simulation with astronomical forcing; instead we just simulated the storm surge component. To justify this choice (which was also followed in many previous studies, e.g. Dullaart et al., 2021), we had previously run a series of sensitivity tests to check if there are significant non-linear interactions between the astronomical tide and storm surge components, which would influence model output of still total water levels in our study region (Horsburgh and Wilson, 2007; Idier et al., 2019). Flood hazard can be underestimated if these non-linear interactions are not accounted for (Williams et al., 2016; Arns et al., 2020). Our sensitivity tests are described in detail in Appendix C and show that non-linear interactions between tide and surge are indeed negligible in this region. Consequently, we ran surge-only simulations. We ran each model simulation on the University of Southamp-

Table 3. Number of baseline and future TCs of each category (using the Saffir–Simpson scale) within the reduced area of the model domain.

Dataset	Tropical storm/depression	1	2	3	4	5
STORM Past/Present	54 255	29 114	14 410	13 003	5938	120
(a) STORM Future: CNRM-CM6-1	31 450	33 595	20 196	19 113	14 762	924
(b) STORM Future: EC-Earth3P-HR	34 018	35 000	19 736	18 254	12 375	657
(c) STORM Future: HadGEM3-GC31-HM	30 409	33 322	20 923	20 202	13 213	491
(d) STORM Future: CMCC-CM2-VHR4	37 685	36 672	18 553	15 911	10 598	621

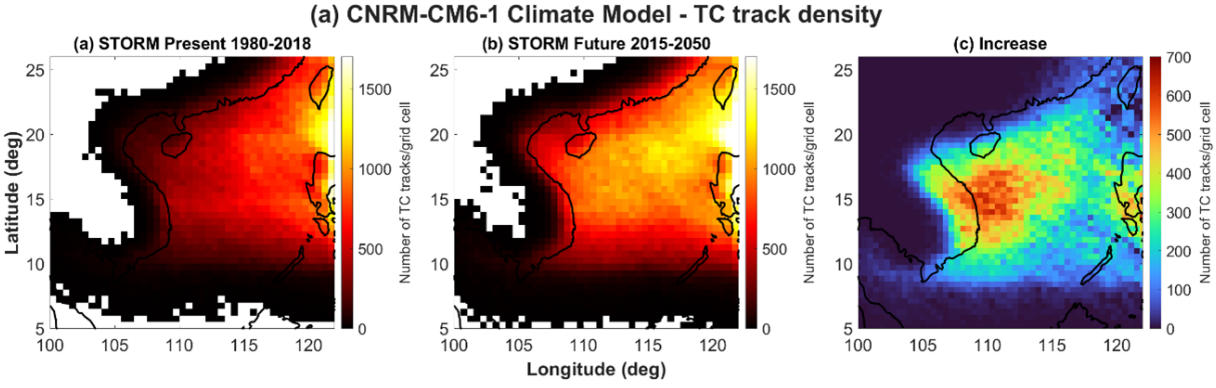

Figure 5. The track density is the number of Saffir–Simpson category 1–5 TC tracks passing through each 0.5° × 0.5° grid cell within each ∼ 35-year period. **(a)** Baseline STORM Past/Present track density of Saffir–Simpson category 1+ (i.e. excluding tropical storms), **(b)** CNRM-CM6-1 climate model – STORM Future track density of Saffir–Simpson category 1+, and **(c)** the cyclone track density difference between them.

ton's IRIDIS 5 high-performance computing facility. On average, each separate TC simulation took around 15 min to complete. For reasons of data economy, we chose to only save predicted storm surge time series, at 10 min temporal resolution, for each TC, at discrete points along the study area coastline only. As a result, we saved model outputs for 3051 coastline model grid points located along the length of the Chinese, Vietnamese, Cambodian, Thai, and Malaysian coastlines in our study domain (green points in Fig. 2a). We automated this whole process. The final output was time series of storm surges at 3051 coastal grid points, for each of the 30 843 baseline and 63 328 future TCs.

3.3 Computation of return periods

Upon completion of all the simulations, the final stage in the analysis was to estimate storm surge and extreme-sea-level probabilities (i.e. return periods) along the study area coastline, representative of the past/present baseline (1980–2018; 30 843 TCs) and future (2015–2050; 63 328 TCs) period. To estimate return periods of extreme storm surges, we employed the following methodology, based on the approach of Haigh et al. (2014). First, for each of the 3051 coastal grid points we calculated the annual storm surge maxima, for both the baseline and future data sub-sets. We were able to do this because the STORM database assigns a synthetic year (from 1 to 10 000) for each TC. On average, there are between 2 and 15 TCs making or approaching landfall within our domain area each STORM year. Note that we used the annual maximum method, as opposed to a peak-over-threshold approach, because our interest is in selecting surge peaks from TC events which are independent of one another (a potentially unsafe assumption for these STORM datasets). Choosing annual maxima data more likely secures this independence requirement, and 10 000 years of annual maxima still provide plentiful data to work with. Second, the annual maxima storm surge levels were then sorted in descending order and given a rank (m). Third, the probability of exceedance (P) was calculated using the following Gringorten formula:

$$P = \frac{(m-a)}{(n+2a)}, \tag{1}$$

where a is scale parameter equal to 0.44, and n is the number of annual maxima observations. The storm surge return period is given as $1/P$. The Gringorten formula was used due to its suitability for extreme value estimation (irrespective of sample size) and previous record in unbiased return period estimation (Guo, 1990). Hence, for each coastal grid point, we calculated storm surge return periods for both the past baseline and future datasets.

We then calculated return periods for total water sea-level return for each of the 3051 coastal grid points. Because nonlinear interactions between tide and storm surge were determined to be negligible for this region (see Appendix C), we

did this by adding surge levels to a randomly selected astronomical tide, accounting for seasonality in TC, and repeating the process in a Monte Carlo framework. The first step was to run a tide-only model simulation, for the year 2019, and save the predicted tidal levels at each of the 3051 coastal grid points, at 10 min intervals. For each coastal grid point, in a second step, we then ran a harmonic analysis on the modelled time series using the MATLAB T-Tide package (Pawlowicz et al., 2002). Using the computed harmonic constituents, we predicted the tides over a longer 19-year period (2003 to 2021), for each coastal grid point. A full 19-year period was used because it encompasses a complete 8.85-year cycle of lunar perigee and 18.6-year lunar nodal cycle, both of which can influence extreme water levels (Haigh et al., 2011; Peng et al., 2019; Baranes et al., 2020).

The third step was then to select a random date from these 19 years of tide data, accounting for seasonality in TCs. Each synthetic TC in STORM has an assigned month. In our study region, the baseline and future synthetic TCs developed largely between May and November, in accordance with the observed record for this region. Because of this it was possible to match each TC (surge) to the correct month in the tide data, preserving TC seasonality. We subsequently allocated each TC a random time, day, and year from the 19-year tidal cycle. For each individual TC, we extracted the height of the astronomical tide at this given time, day, month, and year and combined it with the predicted corresponding storm surge. We then repeated the steps outlined above – i.e. computed annual maximum total water levels at each grid point, ranking these and computing extreme-total-water-level probabilities using the Gringorten formula. To account for uncertainty, we repeated the process 100 times in a Monte Carlo approach, combining each storm surge value with a different tidal level. Hence, for each coastal grid point, this produced 100 total water return period level (RPL) estimates. From these we calculated an average RPL, for each grid point, and for the baseline and future datasets. The 95th percentile confidence intervals around the mean value were also calculated, for baseline and future scenarios, and are shown in our results below.

4 Results

In this section we compare the past and future return periods, first for just the storm surge component (Sect. 4.1) and then for total water levels (i.e. storm surge plus astronomical tide; Sect. 4.2). We also briefly examine the tracks of the TCs that are responsible for generating the largest storm surges in particular locations along the coastline of the case study area (Sect. 4.3).

4.1 Extreme storm surge return period levels

First, we focus on the storm-surge-only results. Return period levels were estimated as described in Sect. 3.3 from the storm surge height output by the model, in metres above the m.s.l. The computed 10 % annual exceedance probability (AEP) (1 in 10 years), 1 % AEP (1 in 100 years), and 0.1 % AEP (1 in 1000 years) return period levels (RPLs) for the baseline past/present scenario (1980–2018) are shown in Fig. 6a, b, and c, respectively. The figures show the model grid point output RPLs along the study coastlines of southern China, Vietnam, Cambodia, Thailand, and Malaysia. As expected, the storm surge RPLs are the lowest along the coastlines of Malaysia and Thailand, which do not typically experience TCs. They then increase moving northwards along the coastline of Cambodia and Vietnam. Storm surge RPLs are the highest along the southern Chinese coast, reaching values of up to 3.5 m, corresponding with a greater frequency of TCs in this area. The shape of the coastline is also shown to have a strong modulating effect on surge RPL, which is especially noticeable for the more extreme events, whereby the modelled surges are typically amplified within the many bays, river mouths, and inlets located along this northern coastline (Jelesnianski, 1972). Another effect of the shape of the shore is seen along Vietnam's central coastline, where storm surge RPLs are substantially lower (e.g. 1 % AEP surge levels there average ~ 0.7 m) compared to the coastlines of northern and southern Vietnam (1 % AEP surge levels average ~ 1.6 and ~ 1.1 m, respectively). The narrow width of the continental shelf in central Vietnam (Fig. 1) acts to reduce surge amplitude, behaviour that is noticeable even for the most extreme surges. The correlation between storm surge height and continental shelf width is a well-documented characteristic (e.g. Pugh and Woodworth, 2014).

The computed 10 %, 1 %, and 0.1 % AEPs for the future scenario (2015–2050), representing the SSP5-8.5 high-emission climate change scenario, and from the CNRM-CM6-1 climate model run, are shown in Fig. 6d, e, and f, respectively. The spatial patterns observed along the coast closely resemble those of the baseline dataset (Fig. 6a, b, and c), but the RPLs are elevated by up to ~ 1 m in some places. The differences between past and future scenarios are shown in Figs. 6g, h, and i for the 10 %, 1 %, and 0.1 % AEPs, respectively. The increase in surge RPLs is the largest along the southern Chinese coast and along the northern and exposed southern Vietnamese coast. For the 1 % AEP level, the increase over time is approximately 0.8 m around the northern and exposed southern Vietnamese coastline (Fig. 6h). The shape of the coastline, specifically a wide and gently sloping continental shelf, and the angle of the cyclone approach contribute to this amplification of surge RPLs around these particular coastlines, notably including around the more vulnerable Red and Mekong River deltas in Vietnam (Fig. 1; Poulose et al., 2018; Bloemendaal et al., 2019; Pandey and Rao, 2019; Ramos-Valle et al., 2020). The great-

est 0.1 % AEP surge level increase exceeds 1.5 m along the Chinese coastline (Fig. 6i). For the 0.1 % AEP, there are also large differences in the coastlines of Cambodia, Thailand, and the northern part of Malaysia. The baseline model outputs indicate that the coastlines of Cambodia, Thailand, and Malaysia are currently relatively unaffected by storm surges linked to the lower-category TCs. This is expected, as these coastlines have historically rarely experienced TC-induced storm surges of magnitude > 10 % AEP. For more probable storm surge events up to the 10 % AEP standard, this relatively unaffected status is predicted to continue into the future too (Fig. 6d). Present-day 10 % AEP storm surge heights along these coastlines average around 0.36 m – and between today and mid-century there appears to be a 0 increase in levels. However, going to more extreme storm surge probabilities in the future scenarios, sections of this coastline are projected to experience storm surges up to 0.6 m (1 % AEP) and 0.8 m (0.1 % AEP) higher than current levels (Fig. 6h and i). In some locations this doubles the current (baseline) storm surge heights.

Looking at the entire study coastline again, the length of coastline that is exposed to 1 % AEP storm surge levels of 2.5 m (∼ 95th percentile), or greater, more than doubles – going from 353 to 930 km total length, between the baseline and future scenarios. For the more extreme 0.1 % AEP outcome, the baseline scenario has approximately 231 km of coastline with a surge RPL of 3.5 m (∼ 95th percentile) or greater, mostly seen in southern China. This length increases in extent, in the future scenario, to around 577 km of coastline – extending into neighbouring coastline in southern China and for the first time including sections of northern and southern Vietnamese coastlines too.

4.2 Extreme total water-level return period levels

Second, we now focus on the total water RPLs, which combine storm surges with astronomical tides, relative to mean sea level (m.s.l.). The computed 10 %, 1 %, and 0.1 % total water-level AEPs are shown in Fig. 7a, b, and c, respectively, for the coastal model grid points along the case study coastline for the baseline past scenario (1980–2018). The spatial patterns observed along the coastline are similar to the surge-only RPLs (Fig. 6a, b, and c). However, total water-level heights are increased, due to the addition of astronomical tides. The largest increases (up to 2 m) are observed along the southern Chinese coastline, the Gulf of Tonkin, southern Vietnam, and southern Thailand, where tidal range is the largest in the study domain. Elsewhere tides add between 0.3 and 1 m.

The computed 10 %, 1 %, and 0.1 % AEPs are shown in Fig. 7d, e, and f, respectively, for the future scenario (2015–2050), representing the SSP5-8.5 climate change scenario, and from the CNRM-CM6-1 climate model run. As expected, the differences match the storm surge changes in Fig. 6d, e, and f, as tides are assumed to remain constant in our approach. In southern Vietnam, the baseline 1 % total water-level AEP is ∼ 1.9 m a.m.s.l. on the exposed east-facing coastline, but in the future scenario this increased to 2.2 m a.m.s.l.: an increase of 0.27 m. Similarly, in northern Vietnam, where the Red River delta is located, the baseline 1 % total water-level AEP is approximately 2.1 m a.m.s.l., and in the future scenario this increases to 2.4 m a.m.s.l. The corresponding increase between the more extreme 0.1 % total water-level AEP baseline and future scenario is around 0.36 m in the north and 0.56 m in the south of Vietnam.

So far in the analysis we have just considered changes in storminess, but the area will also experience a rise in m.s.l. due to climate change. The IPCC's Sixth Assessment Report (Fox-Kemper et al., 2021) projects a relative m.s.l. mean rise (relative to a 1995–2014 baseline) along the coastline of Vietnam of 0.25 m by the year 2050, under the SSP5-8.5 reference scenario (Fox-Kemper et al., 2021; NASA sea-level tool: https://sealevel.nasa.gov/ipcc-ar6-sea-level-projection-tool, last access: 07 September 2021). The associated confidence limits of this relative m.s.l. mean rise (at the 17th and 83rd percentile according to the IPCC methodology) are 0.17 and 0.35 m. The computed 10 %, 1 %, and 0.1 % AEP total water-level RPLs, for the future scenario (2015–2050), with an additional 0.25 m of m.s.l. rise, are shown in Fig. 7g, h, and f, respectively. Adding mean sea-level rise to the future 1 % AEP total water-level RPLs increases these levels to approximately 2.7 m a.m.s.l. for the north of Vietnam and 2.4 m a.m.s.l. for the southern part of Vietnam.

To examine the results in more detail, we display plots of the full range of calculated return periods in Fig. 8 at 12 model grid points spaced equidistant along the Vietnamese and southern Chinese coastline, where significant and spatially varying changes were observed. The past (solid red line) and future (solid green line) total water levels are shown, along with an additional line showing the future total water RPLs with the addition of a 0.25 m a.m.s.l. rise (dashed blue line). In the background of all results are shaded areas showing the 95th percent confidence bounds around the mean of these total water-level results. For future total water RPLs with the addition of relative mean sea-level rise, these confidence bounds have 0.17 m added to the lower bound and 0.35 m added to the upper bound to additionally capture the uncertainty from mean sea-level rise to the year 2050 using IPCC estimates, in the median SSP5-8.5 scenario, for this location. The results shown in Fig. 8 highlight a few things. The first relates to coastal morphology. As mentioned above, water-level RPLs are the lowest around the central Vietnamese coastline (points g, h in Fig. 8), where the narrow continental shelf acts to reduce surge amplitude. In both the baseline and future scenarios within this central zone, the difference between the smallest (20 % AEP, 1 in 5 years) and largest (0.1 % AEP) total water RPL is less than ∼ 0.8 m. This suggests that the amplitude-dampening effect provided by the coastal morphology extends to even the most severe

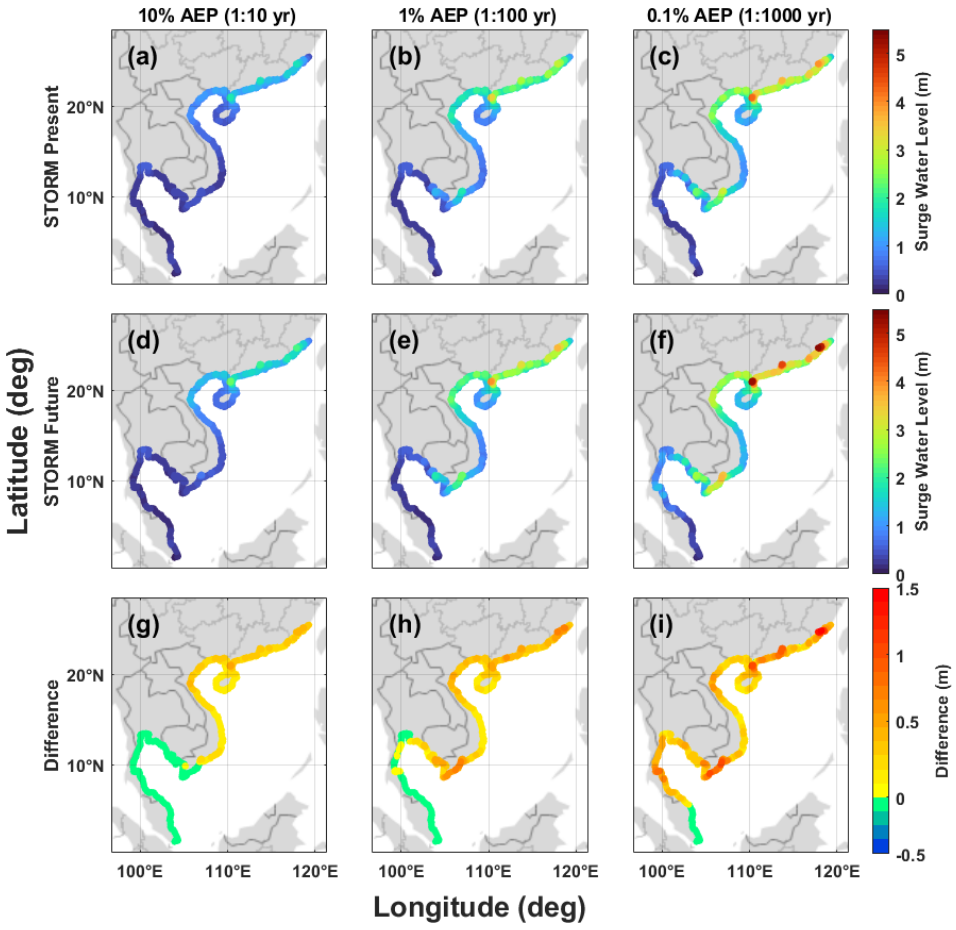

Figure 6. The 10 % AEP **(a, d, g)**, 1 % AEP **(b, e, h)**, and 0.1 % AEP **(c, f, i)** storm surge heights for the Chinese, Vietnamese, Cambodian, Thai, and Malaysian coastlines in the model. First row: STORM baseline data (1980–2018), second row: CNRM-CM6-1 climate model STORM Future data (2015–2050), third row: a difference plot to highlight the areas with the greatest change in surge heights between STORM baseline and STORM Future model results.

storm surges. The second thing of note relates to changes in total water RPLs over time. Along the Vietnamese coastline, the largest differences between the baseline and future scenarios occur along the exposed southern coastline. The future 1 % AEP total water RPL near the Mekong River delta (points j and k in Fig. 8) is 0.6 m higher than the baseline $\sim$ 1 m total water RPL value, while at the northern coastline of Vietnam near the Red River delta (point d in Fig. 8), the total water-level increase over time is only around 0.3 m. The difference is only 0.12 m for the same 1 % AEP return period in the central coastline of Vietnam (points g and h in Fig. 8). The third thing of interest is that at most of the selected 12 grid points the changes in future total water-level return period exceed that of a 0.25 m m.s.l. rise by 2050. This highlights that under the SSP5-8.5 climate change scenario, changes in storminess are likely to dominate over changes in mean sea-level rise in the coming 3 decades. This holds true for the 1 % AEP total water level, and the magnitude of the effect increases as events become more extreme (up to 0.1 % AEP). The exception to this result is along the central coastline of Vietnam where surge amplitudes are consistently reduced, even at extreme probabilities, as discussed previously.

4.3 Cyclone tracks

Finally, we briefly examine the tracks, orientation, and strength of the TC that are responsible for generating the largest storm surges in particular locations along the coastline of the case study area. Tracks of the baseline synthetic TC responsible for the 10 largest modelled storm surges, located at 12 discrete points along the coastline of Vietnam and southern China, are shown in Fig. 9. The different TC categories are shown by different colours. There are clear differences, moving geographically north to south, in the origins and magnitudes of each TC, but what they all have in common is they pass to the south and west of each point as the TCs travel westwards within the domain. This is expected, as the Coriolis effect pushes winds in a cyclonic direction in the Northern Hemisphere, and it is the strong onshore winds

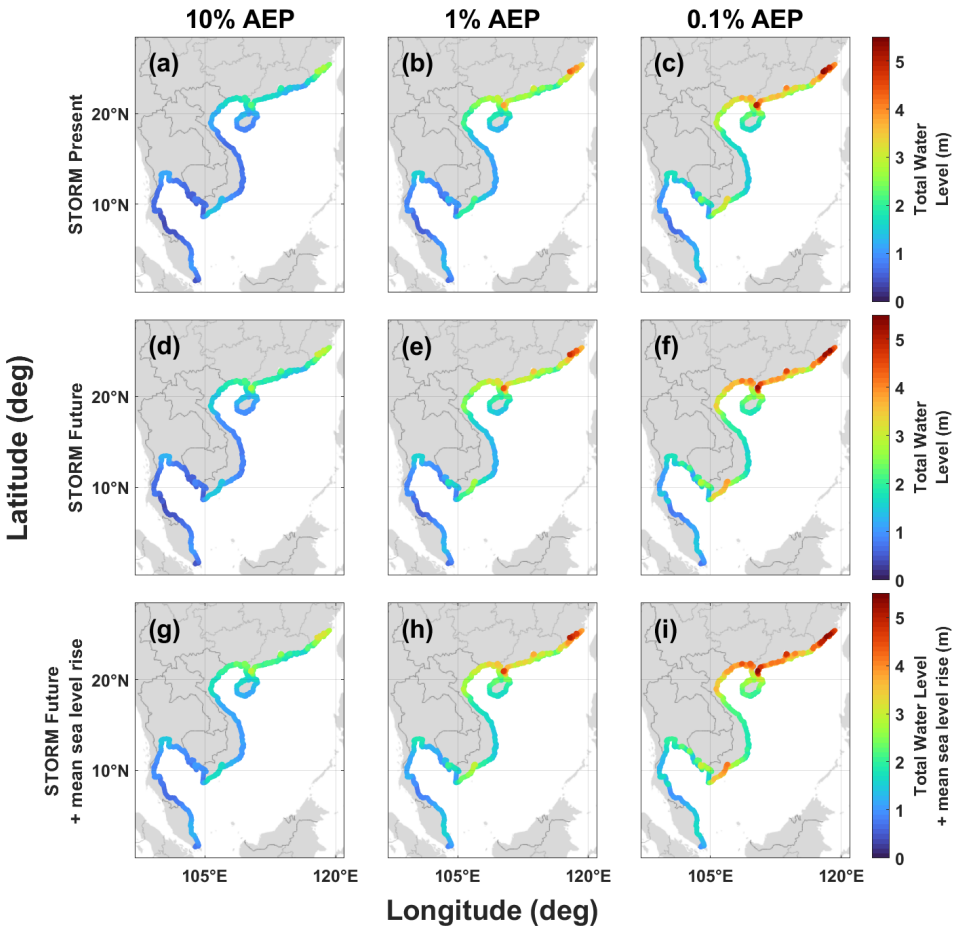

Figure 7. The 10 % AEP **(a, d, g)**, 1 % AEP **(b, e, h)**, and 0.1 % AEP **(c, f, i)** total water level (tide + surge heights for the Chinese, Vietnamese, Cambodian, Thai, and Malaysian coastlines in the model. First row: STORM baseline data (1980–2018), second row: CNRM-CM6-1 climate model STORM Future data (2015–2050) total water levels, third row: CNRM-CM6-1 climate model STORM Future data total water levels with 0.25 m addition for rising mean sea levels up to 2050.

in the first and second cyclone quadrants that are responsible for generating a large part of the storm surge. The TCs that generate the largest storm surges at the northerly points are typically associated with larger-category events (3, 4, and 5), whereas for the southerly points, small-category events (1 and 2) dominate.

5 Discussion

In this paper we forced a hydrodynamic coastal model of the South China Sea with wind and pressure data from a novel database of synthetic baseline and future (SSP5-8.5 – high greenhouse gas emissions) TC activity, representative of 10 000 years of TC activity in each case. Our overall goal was to gain a better understanding of the potential changes to extreme storm surge-level and total water-level probabilities that could occur along the southern Chinese, Vietnamese, Cambodian, Thai, and Malaysian coastlines under a high-emission climate scenario by 2050. This area of Southeast Asia is considered to be a hotspot for projected future sea-level extremes related to intense TC storm activity and contains many densely populated low-lying areas (McGranahan et al., 2007; Nicholls and Cazenave, 2010; Kirezci et al., 2020; Nicholls et al., 2021). Our modelling results show that a projected shift in TC behaviour under a SSP5-8.5 climate scenario would raise surge heights along the lengths of the Chinese and Vietnamese coastlines. By 2050, storm surges along the southern Chinese and Vietnamese coastlines are predicted to be 0.8 m (1 % AEP) and 1.6 m (0.1 % AEP) higher than today. The TC approach angle means that some northern and eastern stretches of coast in the model domain would be orientated to be more vulnerable to storm surges, irrespective of their coastal morphologies, because of funnelling effects within bays and inlets (Pandey and Rao, 2019). However, coastal morphology can modulate surge heights in certain instances too. Despite storm surge heights increasing along the northern and southern Vietnamese coastline by 2050, future storm surges along

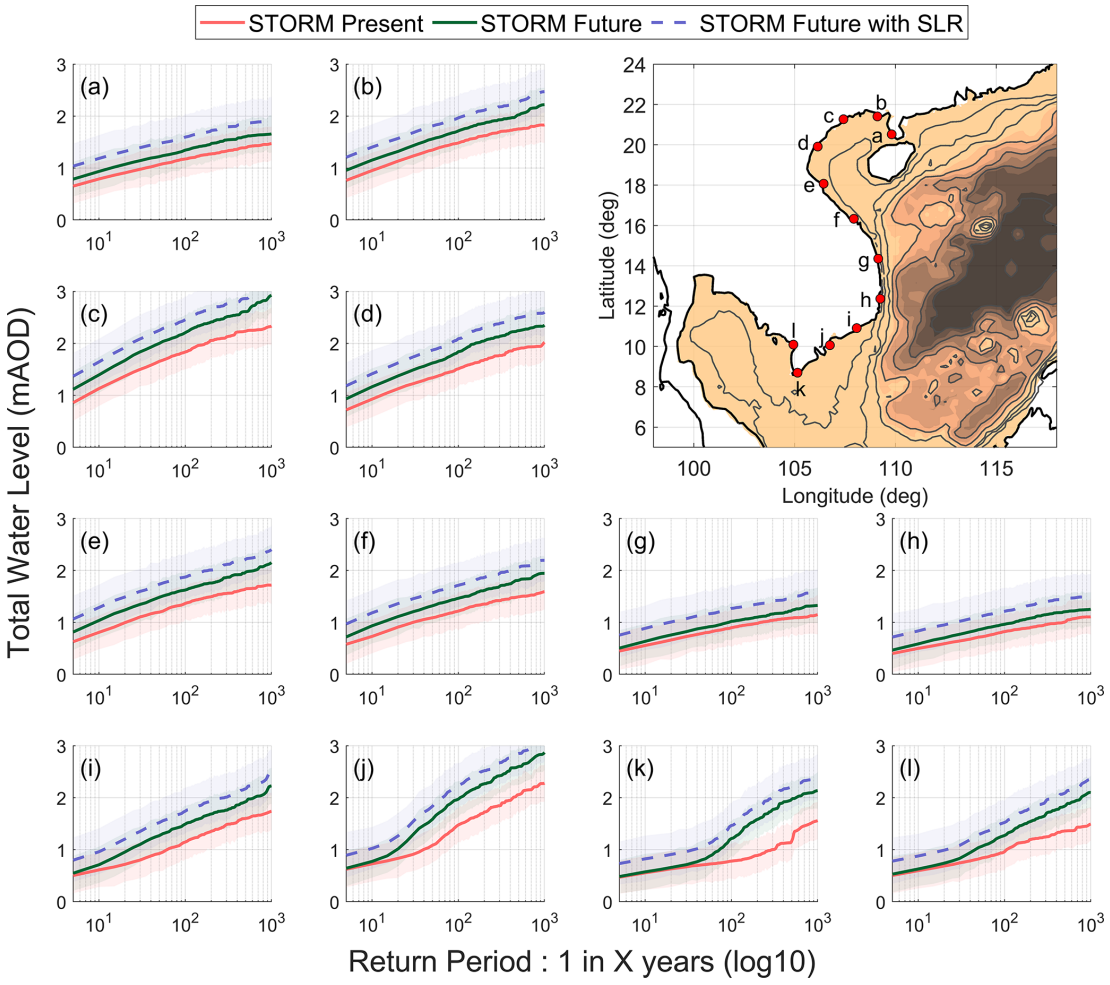

Figure 8. The relationship between past/present baseline (red) and future (green) total water-level return period (log scale, 1 : X years) at equidistant locations at and around the Vietnamese and southern Chinese coastlines. Future return periods with 0.25 mean sea-level rise due to climate change by 2050 are shown with a dashed blue line. Shaded areas indicate the 95th percent confidence level around each mean total water-level return period value.

the central portion of Vietnam's coastline increase much less, even though this section of coastline is the most exposed to increases in the frequency and intensity of TCs that induce storm surges. Surge heights are modulated here because there is no wide and gently sloping continental shelf to amplify storm surge energy, and there are few coastal inlets and river mouths here to funnel and enhance storm surge wave heights (Jelesnianski, 1972; Dube et al., 1981).

One facet of this change suggests that a trend of TCs gradually migrating polewards and achieving their maximum intensity in more northern latitudes is expected to continue into the future (Kossin et al., 2014). This trend is in fact seen in the CNRM-CM6-1 global climate model behind the STORM data used in this analysis, along with an apparent greater number of more intense TCs occurring in the future within the WNP region. Within the smaller limited domain of our South China Sea model, we also see a wider distribution of activity over this region, with an increasing number of strikes to east-facing coastlines (particularly in central Vietnam, Fig. 5c), and even a small number of TCs travelling further southwards. The reasons were not explored but could be due to a seasonal effect; recent research suggests that peak season (July–September) TCs in the WNP are more likely to migrate polewards than later-season (October–December) TCs (Feng et al., 2021).

The model has a variable triangular grid resolution, with greater detail along Vietnam's coastlines. It should be noted that there is potential for sub-optimal accuracy in storm surge levels, particularly within small coastal features such as inlets, bays, or estuaries, where coastal resolution is insufficient for capturing features in detail. For example, Bertin et al. (2014) showed that within small seas wave radiation can induce setup that transforms storm surge levels along exposed coastlines, with even the small waves entering bays

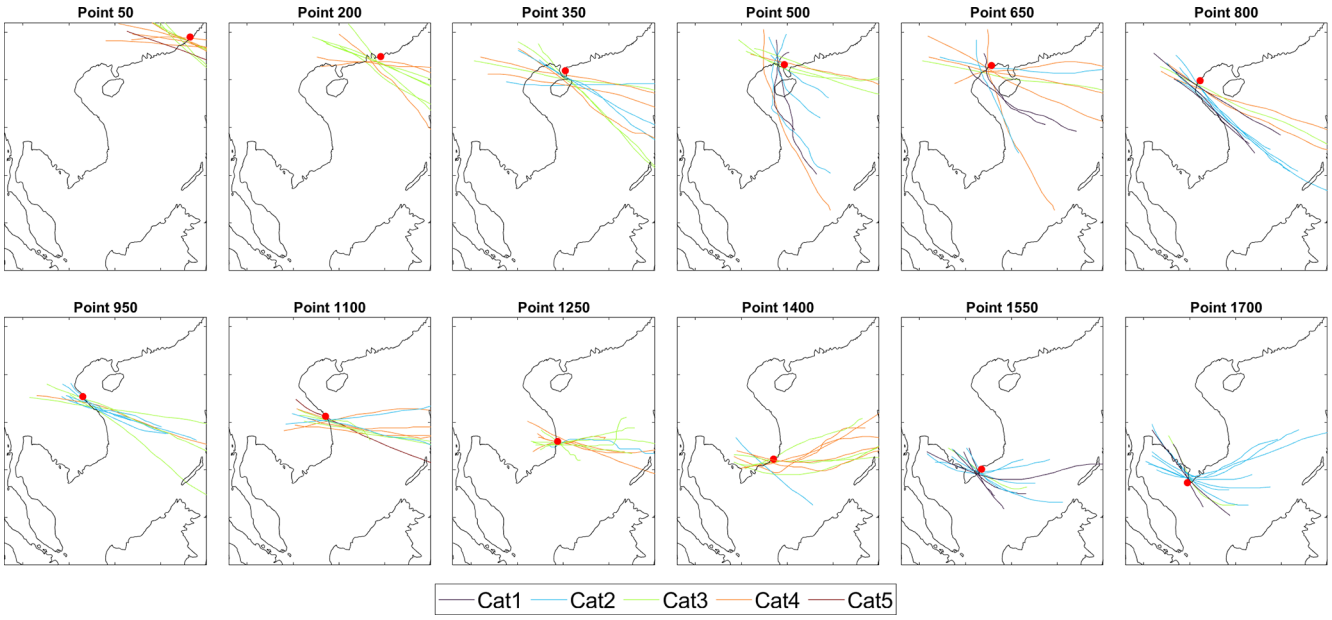

Figure 9. The tracks of the past/present STORM cyclones which produce the 10 largest surges at 12 selected coastal points along the Vietnamese and Chinese coastlines. All demonstrate that it is the onshore winds associated with the TC that are forcing storm surge levels. Before around point 1700 an anticlockwise-turning TC travelling westwards ensures that onshore winds (and thus storm surges) are northeast of the TC and offshore winds southwest. However, after this point, with the coastline curving, onshore winds flip around so that storm surges and onshore winds are southwest of the TC.

and inlets, affecting water levels. Unfortunately, the number of TC simulations entailed in this study meant that there had to be a trade-off between rendering coastal detail and reasonable computational timescales. Future work in such locations, looking at local sections of coastline, would require detailed modelling to estimate extreme water levels due to storm surge. Additionally, currents and wave action are specifically not incorporated in the modelling, as it was outside of the project scope. Such wave models will be a valuable addition to the scientific discussion, as their high spatial resolution at the coastline would ensure that nearshore wave dynamics, such as wave setup, are adequately resolved (Saulter et al., 2017; Melet et al., 2018; Dodet et al., 2019; Hinkel et al., 2021).

Beyond the increased storm surge heights computed along northern Vietnam and southern China, our results suggest that the effects of a changing climate on extreme sea levels will also affect more southerly latitudes around southern Vietnam, Cambodia, and parts of Thailand and Malaysia. This is troubling, as currently extreme sea levels here are rare events. The 10 % AEP storm surge presently averages around 0.36 m along this Vietnamese–Cambodian–Thai portion of coastline. The more extreme 1 % storm surge AEP rarely exceeds 0.5 m along these coastlines, and there is so little storm surge activity that for some sections of Thai and Malaysian coastlines the difference between 10 % AEP and 0.1 % AEP extreme sea levels is under 10 cm. We found that the lowest-impact–highest-probability storm surges (> 10 % AEP) along these coastlines are unlikely to greatly increase in the future. However, more extreme storm surges (1 % AEP to 0.1 % AEP) do increase in the future, under the SSP5-8.5 climate scenario. The worst-hit sections of the Vietnamese–Cambodian–Thai coastline see 1 % AEP storm surge heights increase by 0.6 m (0.8 m for 0.1 % AEP surges). The implications of this are that the flood defences and plans for these previously sheltered coastlines may over time become unfit for their purpose, as a consequence of the projected climate changes in this region leading to TC-induced storm surges.

We also examined what happens to storm surge frequency with TCs occurring with greater intensity in the future. The gap between baseline and future percent AEPs suggests that the extreme storm surge levels we experience today would occur in the future with greater regularity. For example, a 1 % AEP storm surge occurring around Ho Chi Minh City (Fig. 8j) with a height of $\sim$ 1.4 m today (excluding tide and mean sea-level rise contributions) is projected to occur at close to 2.8 % AEP (1 in 35-year return period) in the future, under the SSP5-8.5 climate scenario. Storm surge levels associated with a 1 % AEP event near the Red River delta (Fig. 8d) today would correspond to a 3.3 % AEP (1 in 30-year return period) frequency in the future. The same effect can be observed to varying degrees for all location points plotted, with a greater increase in occurrence observed in the northern/southern parts of the Vietnamese coastline (points a–f and i–l in Fig. 8) than observed in the middle section of the coastline (points g–h in Fig. 8). This substantial in-

crease in frequency suggests that flood defence standards will need to be upgraded at coastal locations, and flood managers will need to consider augmented, alternative, or combined methodologies to cope with more widespread, higher, or more frequent storm surge scenarios. Complex and higher dyke systems alone may be insufficient for storm surge flood hazard. It is also worthwhile to consider that breaches in storm surge defences may coincide and/or combine with pluvial runoff or fluvial flooding after a typhoon or monsoonal rainfall when normal inland flood releases (e.g. drains, flood gates, or flood storage areas) could be unavailable.

A greater number of intense TCs in the future, due to projected climate changes, also more spatially dispersed than today, means not only that extreme sea levels become higher in the future in our study area, but also that the total lengths of coastline experiencing the more extreme storm surges also extend. In our analysis, the highest storm surge levels ($\geq$ 2.5 m in 1 % AEP, $\geq$ 3.5 m in 0.1 % AEP: approximately the 95th percentile of baseline coastal storm surge levels) seen today occurring only along the coastline of southern China are projected to extend further south into Vietnam over the next 30 years. This spread would more than double the length of coastline currently impacted by such high surge levels. In Vietnam, the northern communes have more experience with TCs making landfall with some regularity and coping with TC-induced storm surges. The system of flood defences is better prepared for such eventualities. But at Vietnam's southern coastlines the population is not as well-equipped to withstand extreme-sea-level inundation (Kleinen, 2007; Takagi et al., 2012; Larson et al., 2014; Anh et al., 2017). A significant proportion of the country's total population lives along this low-lying coastline in cities or within its two main deltas: the Red and Mekong River deltas (Dasgupta et al., 2009; Hinkel et al., 2014; GFDRR, 2015; Bangalore et al., 2019; Nicholls et al., 2021). This, alongside the considerable agricultural and infrastructural capital value, explains why these low-lying coastlines are particularly vulnerability to storm surge hazard (Nguyen et al., 2007; Hung et al., 2012; Edmonds et al., 2020). The Mekong River delta has long been identified as being at particular risk of coastal flooding because mean sea levels have historically been rising here at the same time that mean land elevations have been sinking – and sinking at a faster rate than previously realised (Hung et al., 2012; Erban et al., 2014; Dang et al., 2018; Minderhoud et al., 2017; GSO, 2019; Oppenheimer et al., 2019; Nicholls et al., 2021). As one of the most strategically important areas of the entire model domain, we aim to explore the potential impacts of predicted extreme total water levels to the Mekong River delta region in a future paper.

Mean sea-level rise has not been explicitly incorporated in our future model simulations, but it would likely have an amplifying effect on extreme sea levels. To accommodate for the impact of mean sea-level rise for the Vietnamese coastline as an example, we instead simply added a 0.25 m increase on top of the total water-level results (Fig. 8). We find that the projected increases in storm surge heights along the entire Vietnamese coastline in the future, under the SSP5-8.5 climate scenario, can be up to 0.6 m in the 1 % AEP measure (and 0.8 m in the more extreme 0.1 % AEP). Surge heights are even higher along southern Chinese coastlines (Fig. 6h), but even an average of all 1 % AEP surge-level increases along this coastline actually exceeds the anticipated permanent addition due to climate change in local m.s.l. Consequently, storm surge would appear to present a bigger (albeit limited time) hazard to this region than rising m.s.l. by 2050. This is particularly interesting, as past changes in m.s.l. have dominated changes in extreme sea levels in extratropical regions, with mostly negligible changes observed in storm surges (Seneviratne et al., 2012; Marcos et al., 2015; Mawdsley and Haigh, 2016). The results of our study, which highlight the large – and growing – impacts of storm surge flooding, clearly demand an urgent re-evaluation of existing flood risk, defence design, and planning standards to include appropriate focus on the emerging risks posed by climate-driven storm surges. High-value areas south of around 15° latitude, which have historically disregarded the risks posed by current and future storm surges, have the strongest exposure to this risk (Takagi et al., 2012; Anh et al., 2017).

There are factors that influence extreme sea levels (such as wave runup and setup, TC latitude, or seasonality of m.s.l.) that have not been incorporated in our model setup, as they are currently beyond the scope of the project. However, they could easily be incorporated in future analyses. For example, we constructed TCs for the MIKE 21 FM model using the Holland method (Harper and Holland, 1999), but alternative approaches may produce slightly different TC wind and pressure gradients in the model to induce storm surge heights. Naturally, there are also alternative choices that could have been made in our study approach that would or may have altered our findings. For example, we selected a single future STORM scenario (CNRM-CM6-1) out of a possible four climate model outputs, and any biases in this data would also translate into our model results. However, all STORM versions of the averaged 2015–2050 future climate (Table 3) consistently showed an increase in TC intensity, frequency, and altered spatial distribution in the South China Sea region. Future work could compare results across the three other climate simulations to better quantify uncertainty. We also highlight again that waves, particularly wave setup and runup, are important contributors to extreme sea level and coastal flooding, particularly in areas of intense TC activity. Due to the project time, computation outlay, and limit of the budget that funded this study, we have focused in this paper only on storm surges and still sea levels. Future work could include waves. The same framework could be applied to simulate past/present and future wave climates and incorporate them in estimates of total water-level probabilities.

Finally, we stress that in this paper we have utilised the future STORM database from Bloemendaal et al. (2022b) that is based on a SSP5-8.5 climate change scenario. Note that

Bloemendaal et al. (2022a) only created TCs for the SSP5-8.5 scenario and no others, so we were not able to run other climate projections. SSP5-8.5 assumes a future society that has developed within the highest greenhouse gas emissions pathway, being more energy-consumptive but also successfully using innovation and technology to adapt, rather than mitigate, to its environmental problems. It has less social and economic inequality compared to most other pathways and has a booming global economy. A SSP5-8.5 future represents a low-likelihood outcome for 2100 (Hausfather and Peters, 2020; IPCC, 2021; Pielke et al., 2022), and the most plausible scenario for 2100 is thought to be closer to SSP2-4.5 and SSP3-7 if pledges and global climate progress so far are incorporated. Nevertheless, the carbon gap between what we have now and what we ought to achieve by 2050 looms large (Hausfather and Peters, 2020; Pielke et al., 2022). It will require an enormous global effort to achieve the policy goal of global net-zero CO_2 emissions by 2050, not least because this policy relies on decarbonisation technologies for decades to come (IEA, 2022; Pielke et al., 2022). Climate projection outcomes for 2100 are provisional, which means our climate by 2050 is unknown. This uncertainty is also seen in the International Energy Agency's (IEA) research, which suggests that populations in 2050 would be living through an intermediate era, with CO_2 emission levels that have plateaued before levels dip further by 2100 (Lee et al., 2021; IEA, 2022; Pielke et al., 2022). Indeed, Schwalm et al. (2020) argue that the SSP5-8.5 scenario is, in fact, the best tool to quantify physical climate risk by 2050 because this scenario has so far most closely tracked the total cumulative CO_2 emissions to date. Nevertheless, whether SSP5-8.5 represents the future worst-case scenario in global emissions by mid-century or whether it truly characterises the mid-point of global climate on the path to best-case outcomes, SSP5-8.5 outputs have real value when attempting to define future storm surge flood risk response. We therefore believe the model outcomes in this paper provide useful data not only for decision-makers tasked with developing flood policy to serve future generations, but also for sectors thinking about how to develop flood defences that age well because they are capable of withstanding the worst-case scenario storm surges of the future.

6 Conclusions

As the latest IPCC report has indicated (Fox-Kemper et al., 2021), there is currently little ($\sim 20\,\%$) confidence in the scientific community being able to accurately predict future changes to storm surge characteristics, particularly in regions of the world exposed to TCs. The low level of confidence arises both because of the significant challenge of predicting changes in TC activity at a local and regional scale and because relatively few studies have assessed changes in storm surge driven by TCs. Therefore, our overall aim in this paper is to apply a novel modelling framework to more accurately estimate both present and future storm surge and extreme-sea-level hazards, by considering the densely populated coastlines of southern China, Vietnam, Cambodia, Thailand, and Malaysia as a case study.

We configured a depth-averaged hydrodynamic model of the South China Sea and extensively validated it against measured sea-level data from tide gauges in the region. We then forced the hydrodynamic model with 10 000 years of TC activity, representative of a past (1980–2017) and future (2015–2050) period, based on a high-emission climate projection scenario. From the model outputs, we estimate both past and future storm surge and extreme-sea-level probabilities along the coastlines of southern China, Vietnam, Cambodia, Thailand, and Malaysia.

Our results showed that extreme storm surges, and therefore total water levels, increase substantially in the coming decades (up to 2050) under a high-emission (SSP5-8.5) scenario, driven by an increase in the frequency of intense TCs. The increases in storm surges in some regions, e.g. along the southern Chinese and northern and southern Vietnamese coastlines, can exceed ~ 1 m in the 1 % AEP measure, significantly more than the expected changes in mean sea-level rise over this period. The length of coastline that is currently exposed to storm surge levels of 2.5 m or greater more than doubles (353 to 930 km) between the baseline and future high-emission scenario. Around the low-lying and densely populated areas of the Red River and Mekong Delta, storm surges with an AEP of 1 % (1 in 100-year return period) today are likely to see a change in frequency to $\sim 3\,\%$ AEP (1 in 30-year return period) over the coming decades. Furthermore, at higher return periods, the coastlines of Cambodia and parts of Thailand and Malaysia are predicted to experience storm surges induced by TCs in the future scenario, whereas presently they do not. A similar methodology to that applied here could be used to assess changes in storm surges and extreme water levels in other regions of the world that are exposed to TC activity.

Many future projections of extreme sea level, at global, regional, or local scales, only account for changes in relative mean sea level, but here we have shown that changes in storm surges could be significant and even exceed changes in m.s.l. in some areas. Our study area has many low-lying and densely populated coastlines, such as the major river deltas in this region, which are especially vulnerable to storm surges. Given these findings, coastal flood management, planning, and adaptation in these areas should be reviewed for their resilience against changes in storm surges and total water levels in the future.

Appendix A: Flow charts and tables to illustrate model configuration, validation, and simulations

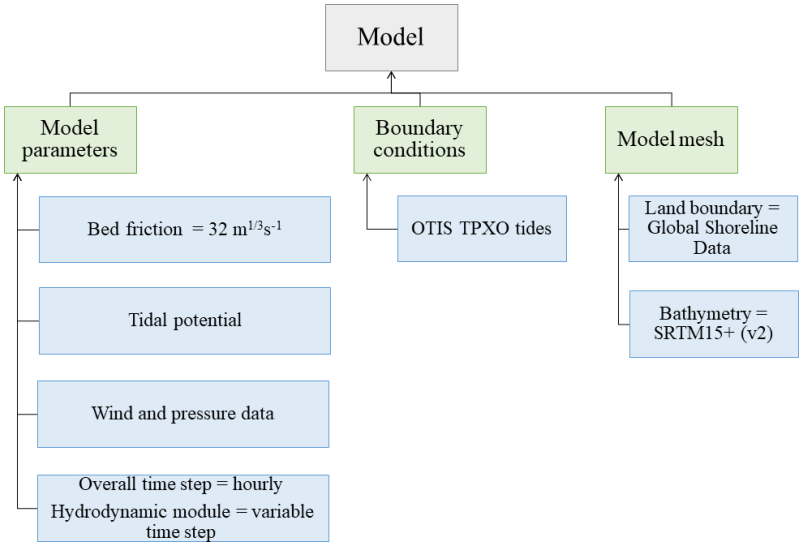

Figure A1. The basic model configuration.

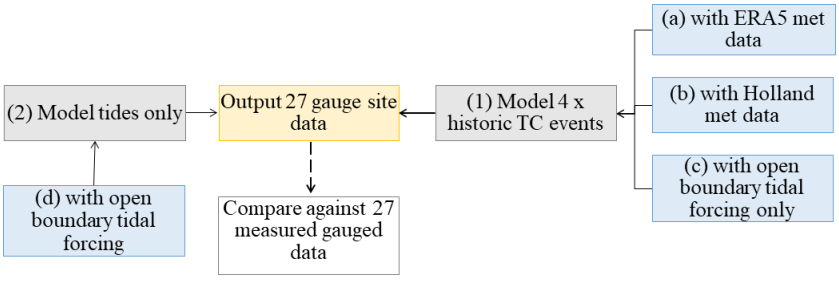

Figure A2. Model validation. The storm surge validation process is described in Sect. 2.3 of the paper; we use different wind and pressure input data to simulate historic TC events, using (1a) ERA5, (1b) the Holland formula, or (1c) no meteorological forcing data. Separately, validation of astronomical tides is illustrated in schematic (2d) with a tides-only model simulation, as described in Sect. 3 below and in Sect. 2.2 of the paper.

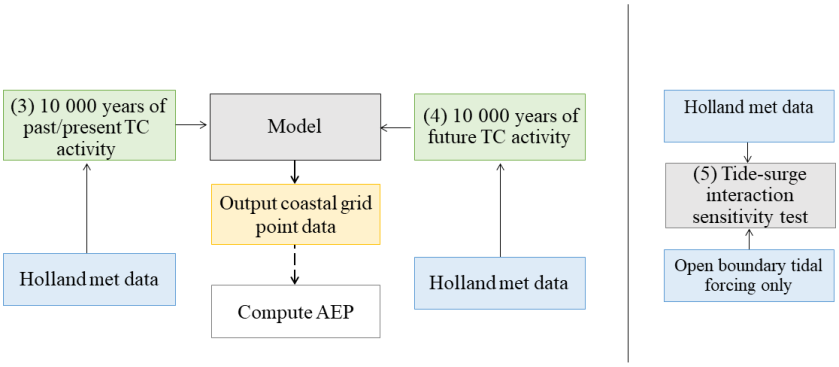

Figure A3. MIKE 21 hydrodynamic model configuration for (3) the past/present scenario, (4) the future scenario, and (5) testing the model sensitivity to tide–surge interactions (see Sect. 3).

Table A1. MIKE 21 FM setup variable and values.

Parameter	Sub-parameter	Description
Time	–	Number of time steps = 5543 Time step interval = 3600 s
Hydrodynamic module	Solution technique (for both the shallow water equations and transport equations)	Time integration = higher order Space discretisation = higher order Minimum time step = 0.01 s Maximum time step = 25 s Critical CFL number = 0.8
	Depth	No depth correction
	Flood and dry	Type = flood and dry Drying depth = 0.01 m Wetting depth = 0.1 m
	Density	Density type = barotropic (default)
	Eddy viscosity	Eddy type = Smagorinsky formulation (default values)
	Bed resistance	Resistance type = Manning number (default) – whole domain Manning number data: format = constant (default) constant value = 32 $m^{1/3}$ s^{-1} (default)
	Coriolis forcing	Coriolis type = varying in domain (default)
	Wind forcing	Files are created as described in the paper
	Ice coverage	No ice coverage (default)
	Tidal potential	Yes, to include tidal potential (default values used)
	Precipitation – evaporation	No precipitation (default) No evaporation (default)
	Infiltration	No infiltration (default)
	Wave radiation	No wave radiation (default)
	Sources	No change (default)
	Structures	No change (default)
	Initial conditions	Constant (default) Initial data surface elevation = 0 m (default) u velocity = 0 m s^{-1} (default) v velocity = 0 ms^{-1} (default)
	Boundary conditions	Seven tidal boundary conditions. Files are created as described in the main paper
	Decoupling	Do not include (default)
	Outputs	Aerial and point data are as described in the paper

Appendix B: Storm surge model validation

Figures B1–B3 below show the simulated storm surges achieved using this approach for Typhoon Sally (September 1996) and Tropical Storm Linda (November 1997), which passed over the southern tip of Vietnam and Mangkhut (September 2018). These results contrast ERA5 (red dashed) and IBTrACS (red dotted) data, at the node point nearest the measured tide gauge location, against measured data (blue). The green vertical line indicates the date and time of the nearest landfall of the TC. Both (a) total water level and (b) surge-only water levels are shown.

Table B1. The mean absolute error (m) between **(a)** measured tide gauge and modelled total water levels and **(b)** tide-removed measured data and modelled surge-only water levels from all the validation hindcast simulations.

Typhoon name (date)	Total water level mean absolute error (m)		Storm-surge-level mean absolute error (m)	
	ERA5 data	Holland model	ERA5 data	Holland model
Sally (September 1996)	0.24	0.21	0.17	0.11
Linda (November 1997)	0.32	0.21	0.26	0.17
Mangkhut (September 2018)	0.25	0.29	0.19	0.11
Ketsana (September 2009)	0.31	0.15	0.24	0.08

Table A1 additionally provides the root mean square difference between measured and modelled total water levels and surge sea levels from these validation simulations (calculated for the number of days shown in Figs. B1–B3).

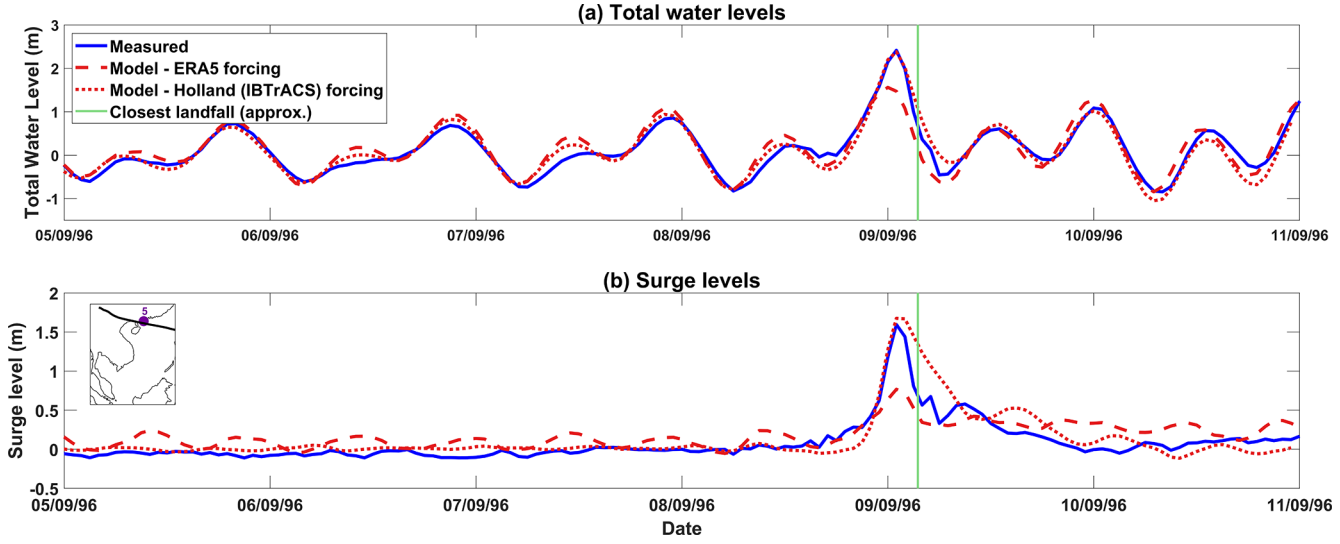

Figure B1. **(a)** Measured and modelled total water levels and **(b)** measured and modelled storm surges at tide gauge 5: Zhapo, China (inset, or see Fig. 1 for location), for Typhoon Sally, which made landfall on 9 September 1996 (green vertical line). Modelled total water level and surges using ERA5 (red dashed) and Holland model (red dotted) wind and pressure fields against measured data (blue).

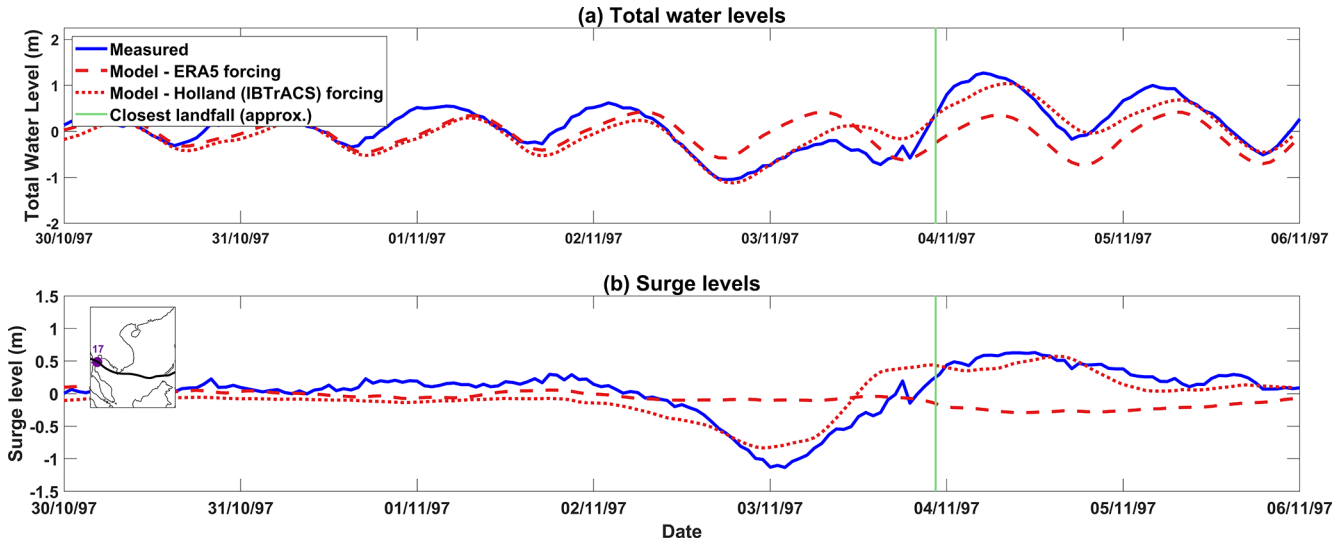

Figure B2. **(a)** Measured and modelled total water levels and **(b)** measured and modelled storm surges at tide gauge 17: Ko Lak, Thailand (inset, or see Fig. 1 for location), for Tropical Storm Linda, which made landfall late on 3 November 1997 (green vertical line). Modelled total water level and surges using ERA5 (red dashed) and Holland model (red dotted) wind and pressure fields against measured data (blue).

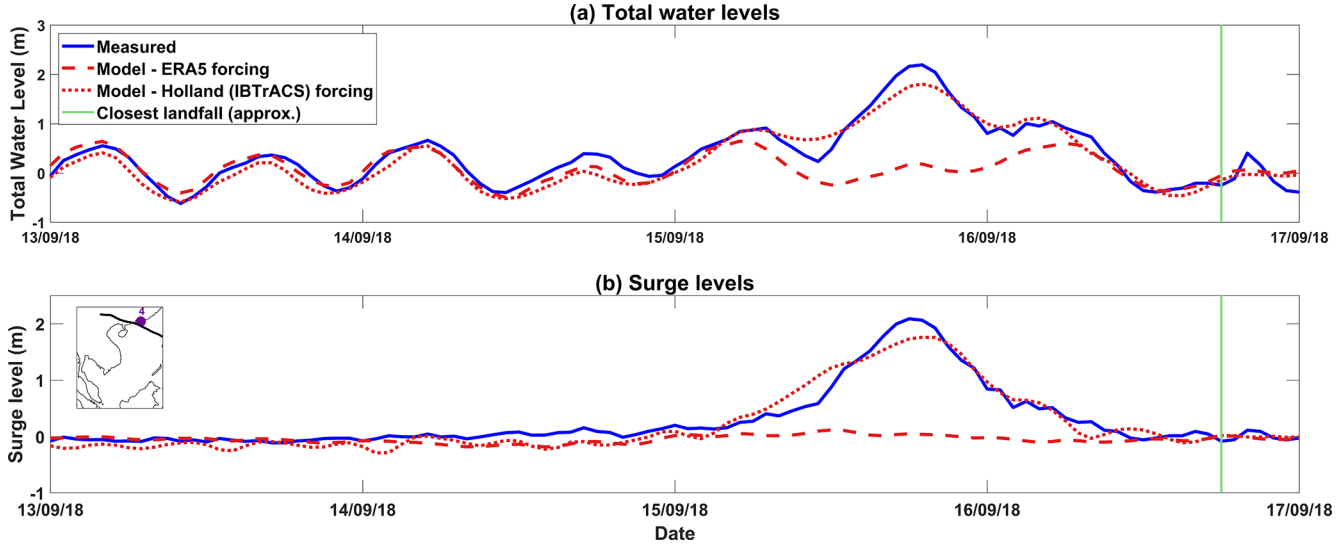

Figure B3. **(a)** Measured and modelled total water levels and **(b)** measured and modelled storm surges at tide gauge 4: Hong Kong, China (inset, or see Fig. 1 for location), for Typhoon Mangkhut, which made landfall in the evening of 16 September 2018 (green vertical line). Modelled total water level and surges using ERA5 (red dashed) and Holland model (red dotted) wind and pressure fields against measured data (blue).

Appendix C: Tide–surge non-linear interaction sensitivity tests

We undertook sensitivity tests to assess whether it was necessary to include the astronomical tide when simulating sea-level conditions for each cyclone. Simulating tides adds the complexity that each cyclone must be randomly assigned a specific day and start time, but STORM only assigns each cyclone to a year and month. Customarily extreme-sea-level modelling studies simulate storm surges separately from the tides and then statistically combine the two to estimate total water-level return periods (e.g. Dullaart et al., 2021). However, this approach ignores the fact that non-linear interactions between the tide and non-tidal components of sea level have been reported for many places around the world and typically result in the highest observed non-tidal residuals occurring around mid tide or low tide rather than at the time of tidal high water (e.g. Horsburgh and Wilson, 2007; Rego and Li, 2010; Mawdsley and Haigh, 2016; Williams et al., 2016; Poulose et al., 2018; Idier et al., 2019). Arns et al. (2020) have recently shown that flood risk can be underestimated if these non-linear interactions are not accounted for, as Haigh et al. (2014) discovered with storm surge errors exceeding 1 m along the Australian coastline, such as when surges were simulated independently of tide for category 5 Tropical Cyclone Rosita (2000).

In our approach to assess the significance of non-linear interactions in this region, the first step was to create model results with meteorological forcing only. We recreated Typhoon Ketsana (2009) using data from the IBTrACS database and the MIKE 21 FM Cyclone Wind Generation tool (DHI, 2017b), with Holland B parameters estimated using the Holland formula (Harper and Holland, 1999). Then, four comparative model runs were undertaken in which the model was driven with both tidal and meteorological forcing. In these four comparative simulations, we shifted the timing of the meteorological forcing so that the peak of the surge occurred (1) around the time of low tide, (2) at the rising tide, (3) at high tide, and (4) at the ebb tide. The results are shown in Fig. C1 and highlight that differences in the height and timing of the simulated surge between tidal and meteorological forcing versus meteorological forcing alone, around the mid-section of Vietnam, are nominal. While the maximum height and duration of the event are not affected, the shape and timing of the surge peak are impacted by as much as 0.25 m and as much as 6 h between high and low tidal states. This influence should be acknowledged. But because this difference is small relative to the Vietnamese tidal range, for simplicity in our study we implemented all hydrodynamic model simulations as meteorological forcing only (surge only), with the intention that results may afterwards be added to a randomly selected maximum tide to compute total water levels and associated return periods.

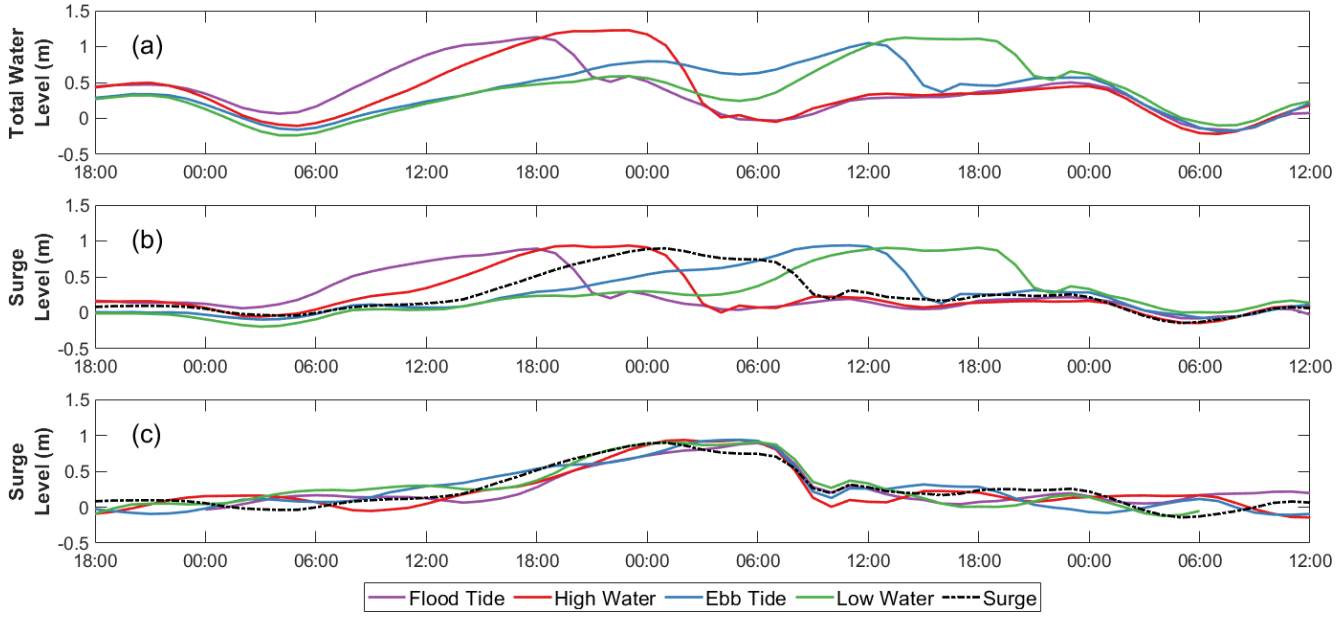

Figure C1. Tide–surge interaction for the Saffir–Simpson scale category 2 Typhoon Ketsana at Son Tra, Vietnam (11 in Fig. 1), which made landfall on 29 September 2009: **(a)** total water levels for low-to-high tide states, **(b)** tide state surge-only levels, and **(c)** tide state surge-only levels adjusted for time offset from peak.

Appendix D: Track density for three alternative climate models to the CNRM-CM6-1 used in this analysis

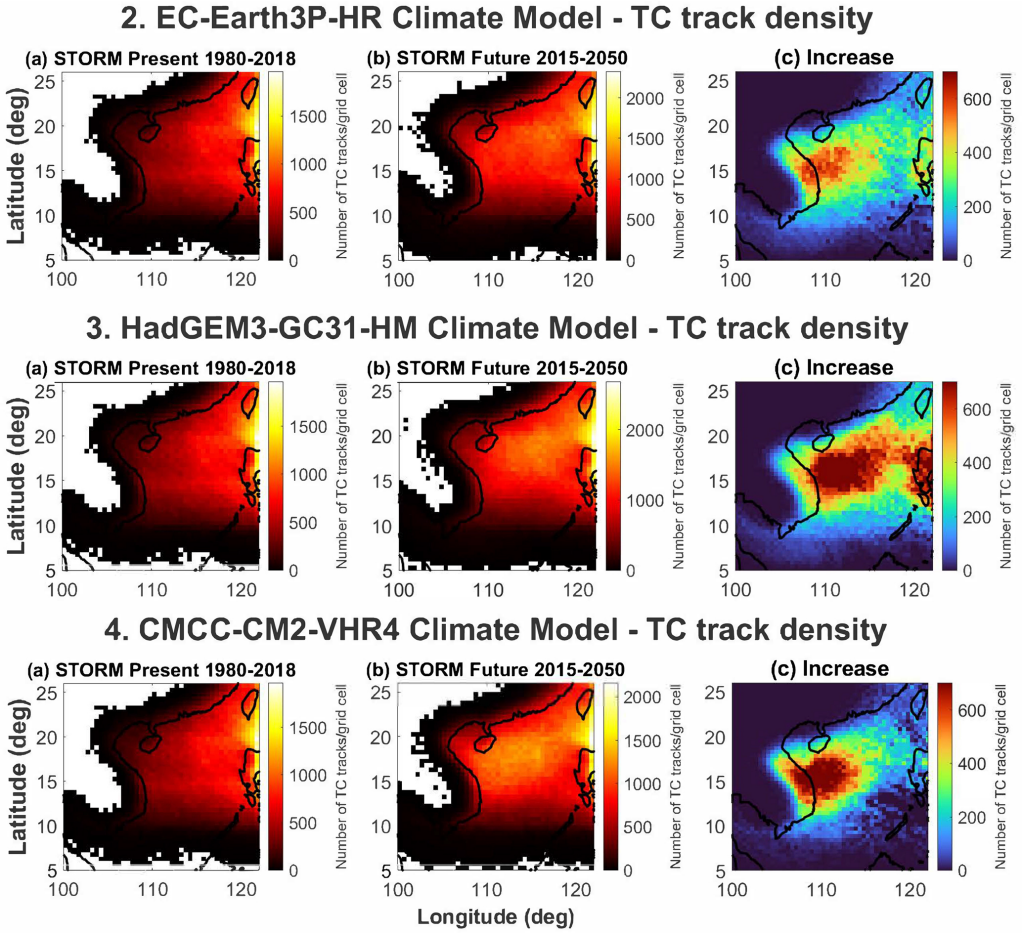

Figure D1. To contrast with Fig. 5 in the paper, here are the number of Saffir–Simpson category 1+ (i.e. excluding tropical storms) TCs that pass through a grid cell over a ∼ 35-year period represented by STORM Past/Present (1980–2018, left column) and STORM Future (2015–2050, central column) for three alternative climate models. Right column: the difference between STORM Past/Present and STORM Future (i.e. the projected increase). **(b)** EC-Earth3P-HR climate model, **(c)** HadGEM3-GC31-HM climate model, and **(d)** CMCC-CM2-VHR4 climate model.

Code and data availability. The past/present and future 10 %, 1 %, and 0.1 % AEP return period storm surge and total water levels for the modelled coastlines of southern China, Vietnam, Cambodia, and parts of Thailand and Malaysia, as described in Sect. 4.1 and illustrated in Fig. 6, are provided for reference in the National Oceanography Centre British Oceanographic Data Centre Published Data Library: https://doi.org/10.5285/e17e7db6-4a78-1a89-e053-6c86abc0253d (Wood et al., 2022).

Author contributions. MW carried out the hydrodynamic modelling simulations, conducted the formal analysis, and prepared the first draft of the manuscript. IDH, SED, and RJN conceptualised this work, designed the methodology, and provided supervision in the UK. IDH further supervised the model design and visualisation. The supervision, methodology development, and resources in Vietnam were provided by TBH and NNH, with formal data analysis carried out by QQL. NB provided key TC resources for this study. All authors commented on and edited the paper prior to submission.

Competing interests. The contact author has declared that none of the authors has any competing interests.

Disclaimer. Publisher's note: Copernicus Publications remains neutral with regard to jurisdictional claims in published maps and institutional affiliations.

Special issue statement. This article is part of the special issue "Coastal hazards and hydro-meteorological extremes". It is not associated with a conference.

Acknowledgements. This work would not have been possible without access to STORM Past/Present and STORM Future datasets (Bloemendaal et al., 2020, 2022). The authors would also like to acknowledge the use of the IRIDIS high performance computing facility, and associated support services, at the University of Southampton in the completion of this work.

Financial support. This work was supported by the UK Natural Environment Research Council (grant no. NE/S003150/1) and, in Vietnam, by the National Foundation for Science and Technology Development (NAFOSTED-RCUK) fund and the Ministry of Science and Technology (Mekong River project, code DTDL-48/18). Nadia Bloemendaal was funded by a VICI grant from the Netherlands Organization for Scientific Research 569 (NWO grant no. 453-13-006) and the ERC Advanced Grant (COASTMOVE (grant no. 884442)).

Review statement. This paper was edited by Francisco Campuzano and reviewed by four anonymous referees.

References

Anh, L. T., Takagi, H., Thao, N. D., and Esteban, M.: Investigation of awareness of typhoon and storm surge in the Mekong Delta – Recollection of 1997 Typhoon Linda, Journal of Japan Society of Civil Engineers, Ser. B3 (Ocean Engineering), 73, I_168–I_173, 2017.

Arns, A., Wahl, T., Wolff, C., Vafeidis, A. T., Haigh, I. D., Woodworth, P., Niehüser, S., and Jensen, J.: Non-linear interaction modulates global extreme sea levels, coastal flood exposure, and impacts, Nat. Commun., 11, 1–9, https://doi.org/10.1038/s41467-020-15752-5, 2020.

Bangalore, M., Smith, A., and Veldkamp, T.: Exposure to floods, climate change, and poverty in Vietnam, Economics of Disasters and Climate Change 3, 79–99, https://doi.org/10.1007/s41885-018-0035-4, 2019.

Baranes, H. E., Woodruff, J. D., Talke, S. A., Kopp, R. E., Ray, R. D., and DeConto, R. M.: Tidally driven interannual variation in extreme sea level frequencies in the Gulf of Maine, J. Geophys. Res.-Oceans, 125, e2020JC016291, https://doi.org/10.1029/2020JC016291, 2020.

Bertin, X., Li, K., Roland, A., Zhang, Y. J., Breilh, J. F., and Chaumillon, E.: A modeling-based analysis of the flooding associated with Xynthia, central Bay of Biscay, Coast. Eng., 94, 80–89, 2014.

Bloemendaal, N., Muis, S., Haarsma, R. J., Verlaan, M., Apecechea, M. I., de Moel, H., Ward, P. J., and Aerts, J. C.: Global modeling of tropical cyclone storm surges using high-resolution forecasts, Clim. Dynam., 52, 5031–5044, 2019.

Bloemendaal, N., Haigh, I. D., de Moel, H., Muis, S., Haarsma, R. J., and Aerts, J. C.: Generation of a global synthetic tropical cyclone hazard dataset using STORM, Sci. Data, 7, 1–12, 2020.

Bloemendaal, N., de Moel, H., Martinez, A. B., Muis, S., Haigh, I. D., van der Wiel, K., Haarsma, R. J., Ward, P., Roberts, M. J., Dullaart, J. C. M., and Aerts, J.: A globally consistent local-scale assessment of future tropical cyclone risk, Science Advances, 8, eabm8438, https://doi.org/10.1126/sciadv.abm8438, 2022a.

Bloemendaal, N., de Moel, H., Martinez, A. B., Muis, S., Haigh, I. D., van der Wiel, K., Haarsma, R. J., Ward, P. J., Roberts, M., Dullaart, J., and Aerts, J. C. J. H. STORM Climate Change synthetic tropical cyclone tracks (Version 1), 4TU, Research Data [Data set], https://doi.org/10.4121/14237678.V1, 2022b.

Calafat, F. M., Wahl, T., Tadesse, M. G., and Sparrow, S. N.: Trends in Europe storm surge extremes match the rate of sea-level rise, Nature, 603, 841–845, 2022.

Caldwell, P. C., Merrifield, M. A., and Thompson, P. R.: Sea level measured by tide gauges from global oceans – the Joint Archive for Sea Level holdings (NCEI Accession 0019568), Version 5.5, NOAA National Centers for Environmental Information [data set], https://doi.org/10.7289/V5V40S7W, 2015.

Chan, J. C.: Interannual and interdecadal variations of tropical cyclone activity over the western North Pacific, Meteorol. Atmos. Phys., 89, 143–152, 2005.

Cid, A., Camus, P., Castanedo, S., Mendez, F., and Medina, R.: Global reconstructed daily surge levels from the 20th Century Reanalysis (1871-2010), Global Planet. Change, 148, 9–21, 2017.

Cid, A., Wahl, T., Chambers, D., and Muis, S.: Storm Surge Reconstruction and Return Water Level Estimation in Southeast Asia for the 20th Century, J. Geophys. Res., 123, 437–451, 2018.

Dang, T. D., Cochrane, T. A., and Arias, M. E.: Future hydrological alterations in the Mekong Delta under the impact of water resources development, land subsidence and sea-level rise, Journal of Hydrology: Regional Studies, 15, 119–133, 2018.

Dasgupta, S., Laplante, B., Meisner, C., Wheeler, D., and Yan, J.: The impact of sea-level rise on developing countries: a comparative analysis, Climatic Change, 93, 379–388, 2009.

Dee, D. P., Uppala, S. M., Simmons, A. J., Berrisford, P., Poli, P., Kobayashi, S., Andrae, U., Balmaseda, M. A., Balsamo, G., Bauer, D. P., and Bechtold, P.: The ERA-Interim reanalysis: Configuration and performance of the data assimilation system, Q. J. Roy. Meteor. Soc., 137, 553–597, 2011.

DHI: MIKE 21 – Flow Model - Hydrodynamic Module, User Guide, https://manuals.mikepoweredbydhi.help/latest/Coast_and_Sea/M21HD.pdf (last access: January 2020), 2017a.

DHI: MIKE 21 Flow Model – Cyclone Wind Generation Tool, Scientific Documentation, https://manuals.mikepoweredbydhi.help/2017/Coast_and_Sea/CycloneTool_Scientific_Doc.pdf (last access: January 2020), 2017b.

Dodet, G., Melet, A., Ardhuin, F., Bertin, X., Idier, D., and Almar, R., The contribution of wind-generated waves to coastal sea-level changes, Surv. Geophys., 40, 1563–1601, 2019.

Dube, S. K., Sinha, P. C., and Rao, A. D.: The effect of coastal geometry on the location of peak surge, Mausam, 33, 445–450, 1982.

Dullaart, J. C., Muis, S., Bloemendaal, N., Chertova, M. V., Couasnon, A., and Aerts, J. C.: Accounting for TROPICAL CYCLONEs more than doubles the global population exposed to low-probability coastal flooding, Communications Earth & Environment, 2, 1–11, 2021.

Edmonds, D. A., Caldwell, R. L., Brondizio, E. S., and Siani, S. M.: Coastal flooding will disproportionately impact people on river deltas, Nat. Commun., 11, 1–8, 2020.

Egbert, G. D. and Erofeeva, S. Y.: Efficient inverse modeling of barotropic ocean tides, J. Atmos. Ocean. Technol., 19, 183–204, 2002.

Emanuel, K.: Response of global tropical cyclone activity to increasing CO_2: Results from downscaling CMIP6 models, J. Climate, 34, 57–70, 2021.

Emanuel, K. A.: Downscaling CMIP5 climate models shows increased tropical cyclone activity over the 21st century, P. Natl. Acad. Sci. USA, 110, 12219–12224, 2013.

Erban, L. E., Gorelick, S. M., and Zebker, H. A., Groundwater extraction, land subsidence, and sea-level rise in the Mekong Delta, Vietnam, Environ. Res. Lett., 9, 084010, https://doi.org/10.1088/1748-9326/9/8/084010, 2014.

Erofeeva, S., Padman, L., and Howard, S. L.: Tide Model Driver (TMD) version 2.5, Toolbox for Matlab, GitHub, https://www.github.com/EarthAndSpaceResearch/TMD_Matlab_Toolbox_v2.5, last access: 9 September 2020.

Feng, X., Klingaman, N. P., and Hodges, K. I.: Poleward migration of western North Pacific tropical cyclones related to changes in cyclone seasonality, Nat. Commun., 12, 1–11, 2021.

Fox-Kemper, B., Hewitt, H. T., Xiao, C., Aðalgeirsdóttir, G., Drijfhout, S. S., Edwards, T. L., Golledge, N. R., Hemer, M., Kopp, R. E., Krinner, G., Mix, A., Notz, D., Nowicki, S., Nurhati, I. S., Ruiz, L., Sallée, J.-B., Slangen, A. B. A., and Yu, Y.: Ocean, Cryosphere and Sea Level Change. In Climate Change 2021: The Physical Science Basis. Contribution of Working Group I to the Sixth Assessment Report of the Intergovernmental Panel on Climate Change, edited by: Masson-Delmotte, V., Zhai, P., Pirani, A., Connors, S. L., Péan, C., Berger, S., Caud, N., Chen, Y., Goldfarb, L., Gomis, M. I., Huang, M., Leitzell, K., Lonnoy, E., Matthews, J. B. R., Maycock, T. K., Waterfield, T., Yelekçi, O., Yu, R., and Zhou, B., Cambridge University Press, Cambridge, United Kingdom and New York, NY, USA, 1211–1362, https://doi.org/10.1017/9781009157896.011, 2021.

GFDRR: Country Profile: Vietnam, https://www.gfdrr.org/en/publication/country-profile-vietnam (last access: 10 December 2020), 2015.

Gray, W. M.: Tropical cyclone genesis, doctoral dissertation, Colorado State University, Libraries, 1975.

Gray, W. M.: Tropical cyclone genesis in the western North Pacific, J. Meteorol. Soc. Jpn., Ser. II, 55, 465–482, 1977.

GSO [General Statistics Office]: General Statistical Office of Vietnam, http://www.gso.gov.vn/, 2019.

Guo, S. L.: A discussion on unbiased plotting positions for the general extreme value distribution, J. Hydrol., 121, 33–44, 1990.

Haigh, I. D., Eliot, M., and Pattiaratchi, C.: Global influences of the 18.61 year nodal cycle and 8.85 year cycle of lunar perigee on high tidal levels, J. Geophys. Res.-Oceans, 116, C06025, https://doi.org/10.1029/2010JC006645, 2011.

Haigh, I. D., MacPherson, L. R., Mason, M. S., Wijeratne, E. M. S., Pattiaratchi, C. B., Crompton, R. P., and George, S.: Estimating present day extreme water level exceedance probabilities around the coastline of Australia: tropical cyclone-induced storm surges, Clim. Dynam., 42, 139–157, 2014.

Haigh, I. D., Pickering, M. D., Green, J. A. M., Arbic, B. K., Arns, A., Dangendorf, S., Hill, D. F., Horsburgh, K., Howard, T., Idier, D., Jay, D. A., Jänicke, L., Lee, S. B., Müller, M., Schindelegger, M., Talke, S. A., Wilmes, S.-B., and Woodworth, P. L.: The tides they are a-Changin': A comprehensive review of past and future nonastronomical changes in tides, their driving mechanisms, and future implications, Rev. Geophys., 57, e2018RG000636, https://doi.org/10.1029/2018RG000636, 2020.

Harper, B. A. and Holland, G. J.: An updated parametric model of the tropical cyclone, in: Proc. 23rd Conf. Hurricanes and Tropical Meteorology, 10–15 January 1999, Dallas, TX, 10–15, 1999.

Harper, B., Hardy, T., Mason, L., and Fryar, R.: Developments in storm tide modelling and risk assessment in the Australian region, Nat. Hazards, 51, 225–238, 2009.

Hausfather, Z. and Peters, G. P., Emissions-the 'business as usual' story is misleading, Nature, 577, 618–621, 2020.

Hersbach, H., Bell, B., Berrisford, P., Hirahara, S., Horányi, A., Muñoz-Sabater, J., Nicolas, J., Peubey, C., Radu, R., Schepers, D., and Simmons, A.: The ERA5 global reanalysis, Q. J. Roy. Meteor. Soc., 146, 1999–2049, 2020.

Hinkel, J., Lincke, D., Vafeidis, A. T., Perrette, M., Nicholls, R. J., Tol, R. S., Marzeion, B., Fettweis, X., Ionescu, C., and Levermann, A.: Coastal flood damage and adaptation costs under 21st century sea-level rise, P. Natl. Acad. Sci. USA, 111, 3292–3297, 2014.

Hinkel, J., Feyen, L., Hemer, M., Le Cozannet, G., Lincke, D., Marcos, M., Mentaschi, L., Merkens, J. L., de Moel, H., Muis, S., and Nicholls, R. J.: Uncertainty and bias in global to regional scale assessments of current and future coastal flood risk, Earth's Future, 9, e2020EF001882, https://doi.org/10.1029/2020EF001882, 2021.

Holland, G. J.: An analytic model of the wind and pressure profiles in hurricanes, Mon. Weather Rev., 108, 1212–1218, 1980.

Horsburgh, K. J. and Wilson, C.: Tide-surge interaction and its role in the distribution of surge residuals in the North Sea, J. Geophys. Res., 112, C08003, https://doi.org/10.1029/2006JC004033, 2007.

Hung, N. N., Delgado, J. M., Tri, V. K., Hung, L. M., Merz, B., Bárdossy, A., and Apel, H.: Floodplain hydrology of the Mekong delta, Vietnam, Hydrol. Process., 26, 674–686, 2012.

Idier, D., Bertin, X., Thompson, P., and Pickering, M. D.: Interactions between mean sea level, tide, surge, waves and flooding: mechanisms and contributions to sea level variations at the coast, Surv. Geophys., 40, 1603–1630, 2019.

Irish, J. L., Resio, D. T., and Divoky, D.: Statistical properties of hurricane surge along a coast, J. Geophys. Res., 116, C10007, https://doi.org/10.1029/2010JC006626, 2011.

IPCC: Summary for Policymakers, in: Climate Change and Land: an IPCC special report on climate change, desertification, land degradation, sustainable land management, food security, and greenhouse gas fluxes in terrestrial ecosystems, edited by: Shukla, P. R., Skea, J., Calvo Buendia, E., Masson-Delmotte, V., Pörtner, H.-O., Roberts, D. C., Zhai, P., Slade, R., Connors, S., van Diemen, R., Ferrat, M., Haughey, E., Luz, S., Neogi, S., Pathak, M., Petzold, J., Portugal Pereira, J., Vyas, P., Huntley, E., Kissick, K., Belkacemi, M., and Malley, J., https://www.ipcc.ch/srccl/chapter/summary-for-policymakers/ (last access: 22 December 2020), in press, 2019.

IPCC: Technical Summary, in: Climate Change 2021: The Physical Science Basis. Contribution of Working Group I to the Sixth Assessment Report of the Intergovernmental Panel on Climate Change, edited by: Masson-Delmotte, V., Zhai, P., Pirani, A., Connors, S. L., Péan, C., Berger, S., Caud, N., Chen, Y., Goldfarb, L., Gomis, M. I., Huang, M., Leitzell, K., Lonnoy, E., Matthews, J. B. R., Maycock, T. K., Waterfield, T., Yelekçi, O., Yu, R., and Zhou, B., Cambridge University Press, Cambridge, United Kingdom and New York, NY, USA, 33–144, https://doi.org/10.1017/9781009157896.002, 2021.

Jelesnianski, C. P.: SPLASH : (Special Program to List Amplitudes of Surges from Hurricanes), I, Landfall storms, United States, National Weather Service, Techniques Development Laboratory, NOAA technical memorandum NWS TDL; 46, https://repository.library.noaa.gov/view/noaa/13509 (last access: January 2021), 1972.

Kirezci, E., Young, I. R., Ranasinghe, R., Muis, S., Nicholls, R. J., Lincke, D., and Hinkel, J.: Projections of global-scale extreme sea levels and resulting episodic coastal flooding over the 21st Century, Scientific Reports, 10, 1–12, 2020.

Kleinen, J.: Historical perspectives on typhoons and tropical storms in the natural and socio-economic system of Nam Dinh (Vietnam), J. Asian Earth Sci., 29, 523–531, 2007.

Knapp, K. R., Kruk, M. C., Levinson, D. H., Diamond, H. J., and Neumann, C. J.: The International Best Track Archive for Climate Stewardship (IBTrACS): Unifying tropical cyclone best track data, B Am. Meteorol. Soc., 91, 363–376, https://doi.org/10.1175/2009BAMS2755.1, 2010.

Knutson, T., Camargo, S. J., Chan, J. C., Emanuel, K., Ho, C. H., Kossin, J., Mohapatra, M., Satoh, M., Sugi, M., Walsh, K., and Wu, L.: Tropical cyclones and climate change assessment: Part II: Projected response to anthropogenic warming, B. Am. Meteorol. Soc., 101, E303–E322, 2020.

Kossin, J. P., Emanuel, K. A., and Vecchi, G. A.: The poleward migration of the location of tropical cyclone maximum intensity, Nature, 509, 349–352, 2014.

Lap, T. Q.: Researching the variation of typhoon Intensities under climate change in Vietnam: A case study of typhoon Lekima, 2007, Hydrology, 6, 51, https://doi.org/10.3390/hydrology6020051, 2019.

Larson, M., Hung, N. M., Hanson, H., Sundström, A., and Södervall, E.: Impacts of Typhoons on the Vietnamese Coastline: A Case Study of Hai Hau Beach and Ly Hoa Beach, in: Coastal Disasters and Climate Change in Vietnam Elsevier, 17–42, ISBN 9780128004791, 2014.

Lee, J.-Y., Marotzke,J., Bala, G., Cao, L., Corti, S., Dunne, J. P., Engelbrecht, F., Fischer, E., Fyfe, J. C., Jones, C., Maycock, A., Mutemi, J., Ndiaye, O., Panickal, S., and Zhou, T.: Future Global Climate: Scenario-Based Projections and Near-Term Information, in: Climate Change 2021: The Physical Science Basis. Contribution of Working Group I to the Sixth Assessment Report of the Intergovernmental Panel on Climate Change, edited by: Masson-Delmotte, V., Zhai, P., Pirani, A., Connors, S. L., Péan, C., Berger, S., Caud, N., Chen, Y., Goldfarb, L., Gomis, M. I., Huang, M., Leitzell, K., Lonnoy, E., Matthews, J. B. R., Maycock, T. K., Waterfield, T., Yelekçi, O., Yu, R., and Zhou, B., Cambridge University Press, Cambridge, United Kingdom and New York, NY, USA, 553–672, https://doi.org/10.1017/9781009157896.006, 2021.

Lin, N. and Emanuel, K.: Grey swan tropical cyclones, Nat. Clim. Change, 6, 106–111, 2016.

Lin-Ye, J., García-León, M., Gràcia, V., Ortego, M. I., Lionello, P., Conte, D., Pérez-Gómez, B., and Sánchez-Arcilla, A.: Modeling of future extreme storm surges at the NW Mediterranean Coast (Spain), Water, 12, 472, https://doi.org/10.3390/w12020472, 2020.

Marcos, M., Calafat, F. M., Berihuete, Á., and Dangendorf, S.: Long-term variations in global sea level extremes, J. Geophys. Res.-Oceans, 120, 8115–8134, https://doi.org/10.1002/2015JC011173, 2015.

Martin, P. J., Smith, S. R., Posey, P. G., Dawson, G. M., and Riedlinger, S. H.: Use of the Oregon State University tidal inversion software (OTIS) to generate improved tidal prediction in the East-Asian Seas, Naval Research Lab Stennis Space Center MS Oceanography Div., https://www7320.nrlssc.navy.mil/pubs/2009/smith1-2009.pdf (last access: July 2023), 2009.

Mawdsley, R. J. and Haigh I. D.: Spatial and temporal variability and long-term trends in skew surges globally, Frontiers in Marine Science, 3, 29, https://doi.org/10.3389/fmars.2016.00029, 2016.

McGranahan, G., Balk, D., and Anderson, B.: The rising tide: assessing the risks of climate change and human settlements in low elevation coastal zones, Environ. Urban., 19, 17–37, 2007.

Melet, A., Meyssignac, B., Almar, R., and Le Cozannet, G., Underestimated wave contribution to coastal sea-level rise, Nat. Clim. Change, 8, 234–239, 2018.

Minderhoud, P. S. J., Erkens, G., Pham, V. H., Bui, V. T., Erban, L., Kooi, H., and Stouthamer, E.: Impacts of 25 years of groundwater extraction on subsidence in the Mekong delta, Vietnam, Environ. Res. Lett., 12, 064006, https://doi.org/10.1088/1748-9326/aa7146, 2017.

Mori, N., Shimura, T., Yoshida, K., Mizuta, R., Okada, Y., Fujita, M., Khujanazarov, T., and Nakakita, E.: Future changes in extreme storm surges based on mega-ensemble projection using 60-km resolution atmospheric global circulation model, Coast. Eng. J., 61, 295–307, 2019.

Mousavi, M. E., Irish, J. L., Frey, A. E., Olivera, F., and Edge, B. L.: Global warming and hurricanes: the potential impact of hurricane intensification and sea level rise on coastal flooding, Climatic Change, 104, 575–597, 2011.

Muis, S., Verlaan, M., Winsemius, H. C., Aerts, J. C., and Ward, P. J.: A global reanalysis of storm surges and extreme sea levels, Nat. Commun., 7, 1–12, 2016.

Muis, S., Apecechea, M. I., Dullaart, J., de Lima Rego, J., Madsen, K. S., Su, J., Yan, K., and Verlaan, M.: A High-resolution global dataset of extreme sea levels, tides, and storm surges, including future projections, Frontiers in Marine Science, 7, 263, https://doi.org/10.3389/fmars.2020.00263, 2020.

Murakami, H. and Sugi, M.: Effect of model resolution on tropical cyclone climate projections, SOLA, 6, 73–76, 2010.

Nicholls, R. J.: Storm surges in coastal areas, in: Natural Disaster Hotspots Case Studies, edited by: Arnold, M., Chen, R. S., Deichmann, U., Dilley, M., Lerner-Lam, A. L., Pullen, R. E., and Trohanis, Z., The World Bank Hazard Management Unit, Disaster Risk Management Series, 6, World Bank, Washington, DC, 79–108, https://doi.org/10.1596/978-0-8213-6332-4, 2006.

Nicholls, R. J. and Cazenave, A.: Sea-level rise and its impact on coastal zones, Science, 328, 1517–1520, 2010.

Nicholls, R. J., Lincke, D., Hinkel, J., Brown, S., Vafeidis, A. T., Meyssignac, B., Hanson, S. E., Merkens, J. L., and Fang, J.: A global analysis of subsidence, relative sea-level change and coastal flood exposure, Nat. Clim. Change, 11, 338–342, 2021.

Nguyen, H. N., Vu, K. T., and Nguyen, X. N.: Flooding in Mekong River Delta, Vietnam, Human Development Occasional Papers (1992–2007), No. HDOCPA-2007-53, Human Development Report Office (HDRO), United Nations Development Programme (UNDP), https://hdr.undp.org/system/files/documents/nguyenhuuninhpdf.pdf (last access: December 2021), 2007.

Oppenheimer, M., Glavovic, B. C., Hinkel, J., van de Wal, R., Magnan, A. K., Abd-Elgawad, A., Cai, R., Cifuentes-Jara, M., DeConto, R. M., Ghosh, T., Hay, J., Isla, F., Marzeion, B., Meyssignac, B., and Sebesvari, Z.: Sea Level Rise and Implications for Low-Lying Islands, Coasts and Communities, in: IPCC Special Report on the Ocean and Cryosphere in a Changing Climate, edited by: Po¨rtner, H.-O., Roberts, D. C., Masson-Delmotte, V., Zhai, P., Tignor, M., Poloczanska, E., Mintenbeck, K., Alegri´a, A., Nicolai, M., Okem, A., Petzold, J., Rama, B., and Weyer, N. M., Cambridge University Press, Cambridge, UK and New York, NY, USA, 321–445, https://doi.org/10.1017/9781009157964.006, 2019.

Pandey, S. and Rao, A. D.: Impact of approach angle of an impinging cyclone on generation of storm surges and its interaction with tides and wind waves, J. Geophys. Res.-Oceans, 124, 7643–7660, 2019.

Pawlowicz, R., Beardsley, B., and Lentz, S.: Classical Tidal Harmonic Analysis Including Error Estimates in MATLAB using T_TIDE, Comput. Geosci., 28, 929–937, 2002.

Peng, D., Hill, E. M., Meltzner, A. J., and Switzer, A. D.: Tide gauge records show that the 18.61-year nodal tidal cycle can change high water levels by up to 30 cm, J. Geophys. Res.-Oceans, 124, 736–749, 2019.

Phan, H. M., Ye, Q., Reniers, A. J., and Stive, M. J.: Tidal wave propagation along The Mekong deltaic coast, Estuar. Coast. Shelf S., 220, 73–98, 2019.

Pielke Jr., R., Burgess, M. G., and Ritchie, J.: Plausible 2005–2050 emissions scenarios project between 2 °C and 3 °C of warming by 2100, Environ. Res. Lett., 17, 024027, https://doi.org/10.1088/1748-9326/ac4ebf, 2022.

Poulose, J., Rao, A. D., and Bhaskaran, P. K.: Role of continental shelf on non-linear interaction of storm surges, tides and wind waves: An idealized study representing the west coast of India, Estuar. Coast. Shelf S., 207, 457–470, 2018.

Pugh, D. and Woodworth, P.: Sea-level science: understanding tides, surges, tsunamis and mean sea-level changes, Cambridge University Press, https://doi.org/10.1017/CBO9781139235778, 2014.

Ramos-Valle, A. N., Curchitser, E. N., and Bruyère, C. L.: Impact of tropical cyclone landfall angle on storm surge along the Mid-Atlantic bight, J. Geophys. Res.-Atmos., 125, e2019JD031796, https://doi.org/10.1029/2019JD031796, 2020.

Rego, J. L. and Li, C.: Nonlinear terms in storm surge predictions: Effect of tide and shelf geometry with case study from Hurricane Rita, J. Geophys. Res., 115, C06020, https://doi.org/10.1029/2009JC005285, 2010.

Saulter, A., Bunney, C., Li, J. G., and Palmer, T.: Process and resolution impacts on UK coastal wave predictions from operational global-regional wave models, in: Proceedings of the 15th International Workshop on Wave Hindcasting and Forecasting and 6th Coastal Hazard Symposium, Liverpool, UK, 10–15 September 2017, 26 pp., 2017.

Schwalm, C. R., Glendon, S., and Duffy, P. B.: RCP8.5 tracks cumulative CO_2 emissions, P. Natl. Acad. Sci. USA, 117, 19656–19657, 2020.

Seneviratne, S.I., Nicholls, N., Easterling, D., Goodess, C., Kanae, S., Kossin, J., Luo, Y., Marengo, J., McInnes, K., Rahimi, M., and Reichstein, M.: Managing the risks of extreme events and disasters to advance climate change adaptation, A special report of working Groups I and II of the Intergovernmental Panel on Climate Change (IPCC), edited by: Field, C. B., Barros, V., Stocker, T. F., Qin, D., Dokken, D. J., Ebi, K. L., Mastrandrea, M. D., Mach, K. J., Plattner, G.-K., Allen, S. K., Tignor, M., and Midgley, P. M., Cambridge University Press, Cambridge, UK, and New York, NY, USA, 582 pp., 2012.

Simpson, R. H. and Saffir, H.: The hurricane disaster–potential scale, Weatherwise, 27, 169–186, 1974.

SwissRe: Industry-first Global Storm Surge Zones, https://www.swissre.com/dam/jcr:dedf399f-af17-4061-928f-dba8229c1499/industry_first_global_storm_surge_zones.pdf (last access: 25 January 2021), 2017.

Tadesse, M. G. and Wahl, T.: A database of global storm surge reconstructions, Scientific Data, 8, 125, https://doi.org/10.1038/s41597-021-00906-x, 2021.

Takagi, H., Thao, N. D., Esteban, M., Tran, T. T., Knaepen, H. L., and Mikami, T.: Vulnerability of coastal areas in southern Vietnam against tropical cyclones and storm surges, in: Proceedings of the 4th International Conference on Estuaries and Coasts (ICEC), Hanoi, Vietnam, 8–11 October 2012, 292–299. 2012.

Takagi, H., Esteban, M., Shibayama, T., Mikami, T., Matsumaru, R., De Leon, M., Thao, N. D., Oyama, T., and Nakamura, R.: Track analysis, simulation, and field survey of the 2013 Typhoon Haiyan storm surge, J. Flood Risk Manag., 10, 42–52, 2017.

Tozer, B., Sandwell, D. T., Smith, W. H. F., Olson, C., Beale, J. R., and Wessel, P.: Global bathymetry and topography at 15 arc sec: SRTM15+, Earth and Space Science, 6, 1847–1864, 2019.

Vitousek, S., Barnard, P. L., Fletcher, C. H., Frazer, N., Erikson, L., and Storlazzi, C. D.: Doubling of coastal flooding frequency within decades due to sea-level rise, Scientific Reports, 7, 1–9, 2017.

Vousdoukas, M. I., Voukouvalas, E., Annunziato, A., Giardino, A., and Feyen, L.: Projections of extreme storm surge levels along Europe, Clim. Dynam., 47, 3171–3190, 2016.

Wahl, T. and Chambers, D. P.: Climate controls multidecadal variability in US extreme sea level records, J. Geophys. Res.-Oceans, 121, 1274–1290, 2016.

Wahl, T., Haigh, I. D., Nicholls, R. J., Arns, A., Dangendorf, S., Hinkel, J., and Slangen, A. B.: Understanding extreme sea levels for broad-scale coastal impact and adaptation analysis, Nat. Commun., 8, 1–12, 2017.

Williams, J., Horsburgh, K. J., Williams, J. A., and Proctor, R. N. F.: Tide and skew surge independence: new insights for flood risk, Geophys. Res. Lett., 43, 6410–6417, https://doi.org/10.1002/2016GL069522, 2016.

Wood, M. L., Haigh, I. D., Quan, L., Hung, N., Darby, S. E., Marsh, R., Skliris, N., Hirschi, J., Nicholls, R. J., and Bloemendaal, N.: Modelled storm surge and total water level return periods along the coastline of China, Vietnam, Cambodia and Thailand (1980–2050), NERC EDS British Oceanographic Data Centre NOC [data set], https://doi.org/10.5285/e17e7db6-4a78-1a89-e053-6c86abc0253d, 2022.

Woodruff, J. D., Irish, J. L., and Camargo, S. J.: Coastal flooding by tropical cyclones and sea-level rise, Nature, 504, 44–52, 2013.

Wong, P. P., Losada, I. J., Gattuso, J.-P., Hinkel, J., Khattabi, A., McInnes, K. L., Saito, Y., and Sallenger, A.: Coastal systems and low-lying areas, in: Climate Change 2014: Impacts, Adaptation, and Vulnerability. Part A: Global and Sectoral Aspects. Contribution of Working Group II to the Fifth Assessment Report of the Intergovernmental Panel on Climate Change, edited by: Field, C. B., Barros, V. R., Dokken, D. J., Mach, K. J., Mastrandrea, M. D., Bilir, T. E., Chatterjee, M., Ebi, K. L., Estrada, Y. O., Genova, R. C., Girma, B., Kissel, E. S., Levy, A. N., MacCracken, S., Mastrandrea,P.R., and White (eds.)], L.L., Cambridge University Press, Cambridge, United Kingdom and New York, NY, USA, 361–409, ISBN 978-1-107-64165-5, 2014.

Zhang, X. and Church, J. A.: Sea level trends, interannual and decadal variability in the Pacific Ocean, Geophys. Res. Lett., 39, https://doi.org/10.1029/2012GL053240, 2012.

Zhang, B. and Wang, S.: Probabilistic characterization of extreme storm surges induced by tropical cyclones, J. Geophys. Res.-Atmos., 126, e2020JD033557, https://doi.org/10.1029/2020JD033557, 2021.